

# SBP-FDEC: Summation-by-Parts Finite Difference Exterior Calculus

Daniel Bach<sup>a,\*</sup>, Andrés M. Rueda-Ramírez<sup>b</sup>, Eric Sonnendrücker<sup>c,d</sup>, David C. Del Rey Fernández<sup>e</sup>, Gregor J. Gassner<sup>a</sup>

<sup>a</sup>University of Cologne, Germany

<sup>b</sup>Universidad Politécnica de Madrid, Spain

<sup>c</sup>Max Planck Institute for Plasma Physics, Germany

<sup>d</sup>Technical University of Munich, Germany

<sup>e</sup>University of Waterloo, Canada

---

## Abstract

We demonstrate that we can carry over the strategy of Finite Element Exterior Calculus (FEEC) to Summation-by-Parts (SBP) Finite Difference (FD) methods to achieve divergence- and curl-free discretizations. This is not obvious at first sight, as for SBP-FD no basis functions are known, but only values and derivatives at points. The key is a remarkable analytic relationship that enables us to construct compatible operators using integral and nodal degrees of freedom. Pre-existing SBP-FD matrix operators can then be used to obtain nodal values from the integral degrees of freedom to derive a scheme with the desired properties.

*Keywords:* Finite Differences, Finite Element Exterior Calculus, Summation-by-Parts, Divergence free, Structure preserving schemes

---

## 1. Introduction

The theory of Finite Element Exterior Calculus (FEEC) by Arnold, Falk, and Winther [1, 2], Arnold [3], with foundational contributions by Monk [4], is a state-of-the-art finite element framework that uses the structure of the de Rham cohomology to preserve topological structures, such as the cohomology groups of the region, or manifold, on which the Partial Differential Equations (PDEs) in question are posed. The primary example used in these foundational papers is the Hodge-Laplacian, but another major application of this framework are problems where an exactly divergence- or curl-free solution is needed. For

---

\*Corresponding author

Email addresses: [daniel.bach@uni-koeln.de](mailto:daniel.bach@uni-koeln.de) (Daniel Bach), [am.rueda@upm.es](mailto:am.rueda@upm.es) (Andrés M. Rueda-Ramírez), [eric.Sonnendruecker@ipp.mpg.de](mailto:eric.Sonnendruecker@ipp.mpg.de) (Eric Sonnendrücker), [ddelreyfernandez@uwaterloo.ca](mailto:ddelreyfernandez@uwaterloo.ca) (David C. Del Rey Fernández), [ggassner@uni-koeln.de](mailto:ggassner@uni-koeln.de) (Gregor J. Gassner)

instance, FEEC has been used to satisfy the divergence-free condition of the magnetic field when discretizing the time-dependent Maxwell's equations (see, for instance, [4] and [3]) and Vlasov–Maxwell equations (see, for instance [5, 6]). The theory has also been applied to other PDEs that need to satisfy divergence constraints, such as the incompressible Navier–Stokes equations. See, for example, Palha et al. [7] or Carlier et al. [8]. In FEEC, compatible ansatz spaces and projections are used to discretize the PDEs. For that purpose, two (for 1D), three (for 2D), or four (in 3D) discrete spaces and conforming projections onto these spaces are necessary to discretize the de Rham cochain complex. The FEEC framework has also recently been extended to broken spaces, such that only local mass matrices are needed [9].

In the literature, a variety of different ansatz spaces and projections have been proposed to discretize the de Rham cochain complex, most of which are polynomial or piecewise polynomial in nature. Classical examples include Nédélec spaces of the first and second kind [10, 11], Whitney forms [12] or Raviart–Thomas elements [13]. These predate the formulation of the FEEC framework. More recently, spline elements using a tensor-product ansatz on hexahedral spaces have also been used, for example, in Buffa et al. [14] and Evans et al. [15].

These approaches differ not only in the choice of finite element spaces, but also in the projection operators they employ, which leads to variations in the associated degrees of freedoms and basis functions of each approach. For instance, the approach of Gerritsma [16] and Gerritsma et al. [17], which motivated the present work, uses nodal and integral degrees of freedom on a one-dimensional subgrid per element. Using tensor products, this construction extends to nodal, line-integral, area-integral, and volume-integral degrees of freedom on a multi-dimensional level. Other approaches, as in Nédélec [10, 11], use higher moment degrees of freedom instead of a subgrid approach.

There is a rich literature of discrete operators on finite-difference-like degrees of freedom using discrete derivative operators to mimic the de Rham complex discretely to achieve similar structure preserving properties as FEEC. These schemes are also known as mimetic finite-difference methods. One survey paper by Lipnikov et al. [18] gives a comprehensive overview of these methods. An early example of such schemes is given in the book of Samarskii [19]. Another important work is the method of Yee [20] for Maxwell's equations, which is the foundation for the class of finite-difference time-domain methods. It uses a staggered space-time grid for the different fields, which automatically preserves the divergence condition of the magnetic field. Another approach of Hyman and Shashkov in [21, 22] and [23] uses the derivation of discrete analogues for the **grad**, **curl**, and **div** operators and their adjoints. In addition to the natural operators, which are these discrete analogues, arising in this context, mimetic discretizations rely on a reconstruction operator to compute point values of the different fields involved. For high-order mimetic finite differences, these are mostly interpolation operators based on the degrees of freedoms in the neighboring cells, as for example in high-order finite volume reconstructions. In [24] a mimetic method on staggered grids is developed for the Vlasov–Maxwell equa-

tions, where the reconstructions are defined by a sliding stencil of Lagrange interpolation or histopolation using the neighboring cells.

A different class of finite-difference methods, called Summation-by-Parts Finite Differences (SBP-FD), introduced Kreiss and Scherer [25] with key theoretical contributions from Strand [26], were developed to re-create energy estimates of classic Finite-Element Methods (FEM). SBP operators use a discrete norm (mass) matrix together with a derivative matrix that operate on nodal degrees of freedom. These operators are constructed such that they mimic integration by parts discretely, enabling the derivation of discrete energy estimated, see Olsson in [27, 28], and entropy estimates, see for instance Crean et al. [29] or Carpenter et al. [30]. A defining feature of these methods is the equivalence of their strong and weak formulations, which is central to obtaining stability results.

These schemes can be extended to a multi-element formulation with the Simultaneous Approximation Term (SAT) approach, treating interface and boundary conditions weakly. For further information, see, for instance, the review papers [31, 32]. SBP operators for the first and second derivative have also been developed for non-polynomial approximation spaces, for instance for trigonometric functions or radial basis functions, see Glaubitz et al. [33, 34]. The SBP framework has also influenced methods beyond finite-difference schemes. One example of this is the Discontinuous Galerkin Spectral Element Method (DGSEM) using a Legendre–Gauss–Lobatto (LGL) grid, see Kopriva [35], where the mass and derivative matrices form an SBP operator, Gassner [36].

Because classical SBP-FD methods rely solely on nodal degrees of freedom and a discrete first-order derivative operator acting on those nodes, it is not immediately clear how to extend them analogously to FEEC to achieve similar structure-preserving properties. Motivated by the analogy between classic nodal FEM and SBP-FD schemes used to mimic the energy analysis, the central question of this paper is whether it is possible to develop a Summation-by-Parts Finite Difference Exterior Calculus (SBP-FDEC) analogous to FEEC. The major scientific obstacle to overcome lies in the fact that, when using only nodal DOFs (SBP-FD), without known analytic basis functions, it is not obvious how to derive discrete derivative operators and projections that satisfy a discrete de Rham cohomology.

To address this issue, we exploit important connections between DGSEM-LGL and SBP-FD, and borrow important ingredients from the work of Gerritsma [17] and Gerritsma et al. [16], who developed FEEC operators using LGL spectral element operators. In Gerritsma et al.’s approach, a subgrid structure is imposed on each LGL element, accompanied by two compatible polynomial spaces and two projection operators in 1D: (i) the polynomial interpolation space and (ii) the polynomial *histopolation* space.

In this paper, we show that, although the histopolation basis polynomials are derived from the LGL Lagrange basis functions, their nodal values depend solely on the (discrete) nodal derivative values of the Lagrange basis. This important observation and the close relationship between LGL spectral element operators and SBP-FD leads us to the central idea of this work: it is possible

to use nodal values like classical SBP-FD operators, while simultaneously accessing sub-grid interval DOFs like in the work of Gerritsma et al. The interval DOFs can be converted back into nodal values by using the derivative matrix of the standard SBP-FD derivative operator, which can be accomplished without requiring explicit basis functions.

This strategy enables us to invoke the fundamental theorem of calculus to construct a discrete complex that is compatible with the de Rham complex, while still performing numerical computations with existing SBP-FD operators using nodal values derived from the integral DOFs. The extension to 2D and 3D via a tensor product ansatz is then straightforward, and when the SBP-FD operator grid contains the boundary nodes, it is also easy to extend the method to multiple elements. Overall, we are able to derive the class of SBP-FDEC schemes.

The remainder of the paper is organized as follows. In section 2, we revisit and generalize the ansatz of Gerritsma [16] to the SBP-FD framework. We include extensions to multiple elements and derivations of discrete 2D and 3D derivative operators based on existing SBP-FD operators. In section 3, we apply this theory to the 2D transverse electric homogeneous Maxwell's equation to demonstrate the capability of the SBP-FDEC to exactly preserve the divergence-free electric field. In section 4, we derive the weak and strong form of the SBP-FDEC method for the Maxwell's equations on a periodic domain and prove the discrete divergence-free property and semi-discrete energy conservation, which can then be extended to fully discrete energy conservation using appropriate established time-integration methods. In section 5, we numerically verify our method on a periodic test case, showing the experimental order of convergence fitting to the established SBP-FD operators, demonstrating that the expected convergence rate is obtained as well as that the scheme is discretely divergence-free and energy preserving. The last section concludes the paper.

## 2. Mimetic Finite Difference Operators

### 2.1. 1D Basis Functions

Our goal in this section is to construct discrete spaces  $U_l$  and  $U_h$  and compatible projections  $p^0$  and  $p^1$  to obtain a discrete 1D de Rham complex, so that the diagram of Fig. 1 commutes. This means, that we get the same result if we first apply the derivative operator  $\frac{\partial}{\partial x}$  and then  $p^1$  or first  $p^0$  and then  $\frac{\partial}{\partial x}$ , and we also get the same result if we first apply  $\frac{\partial}{\partial x}$  and then  $R^1$  or first  $R^0$  and then  $\Delta$ , where  $R^0$  and  $R^1$  are reduction operators, mapping functions to the vector of their DOFs. The discrete de Rham complex ensures, that our spaces are compatible with the derivative operator  $\frac{\partial}{\partial x}$ . This we can later extend with a tensor product ansatz to 2D and 3D to obtain spaces and projections compatible with the **curl** and **div** operators, to achieve divergence-free discretizations.

To obtain such a discrete complex, we will generalize the ansatz proposed by Gerritsma [16], who derives two compatible polynomial spaces using nodal and integral degrees of freedom on a given grid. Instead of using polynomial

spaces, however, we assume an unknown general Lagrange basis that we only know through discrete nodal function values and the corresponding discrete nodal derivative values. This assumption allows us to connect nodal function values to a new set of discrete integral degrees of freedom and further derive corresponding discrete representations and matrix operators.

With this, we are able to derive a discrete de Rham complex, shown in Fig. 1, on the spaces of the nodal and integral DOFs respectively.

$$\begin{array}{ccc}
H^1 & \xrightarrow{\frac{\partial}{\partial x}} & L^2 \\
\downarrow p^0 & & \downarrow p^1 \\
U_l & \xrightarrow{\frac{\partial}{\partial x}} & U_h \\
\downarrow R^0 & & \downarrow R^1 \\
\mathbb{R}^{N+1} & \xrightarrow{\Delta} & \mathbb{R}^N
\end{array}$$

Figure 1: Discrete de Rham complex in 1D.

Let  $\{x_i\}_{i=0}^N$  be a grid in the interval  $I$  with  $x_0 = a$  and  $x_N = b$  and let  $\{l_i\}_{i=0}^N$  be functions in  $C^1([a, b])$ , which fulfill the Lagrange property for the grid points,

$$l_i(x_j) = \delta_{i,j} \quad \forall i, j \in \{0, \dots, N\}, \quad (1)$$

where  $\delta_{i,j}$  is the Kronecker delta. In addition, let  $U_l$  be the span of the Lagrange functions  $\{l_i\}_{i=0}^N$ . We demand that both the constant and linear functions are contained in  $U_l$  to ensure that both  $U_l$  and its derivative space contain the constant functions. This is equivalent to the conditions

$$\sum_{i=0}^N l_i(x) = 1, \quad \forall x \in [a, b], \quad (2)$$

$$\sum_{i=0}^N x_i l_i(x) = x, \quad \forall x \in [a, b]. \quad (3)$$

Since we need to calculate the derivatives, we want a basis representation for  $U_h := \frac{\partial}{\partial x}(U_l)$ . For this, let  $\{h_i\}_{i=1}^N$  be the functions in  $C^0([a, b])$  defined by

$$h_i = - \sum_{j=0}^{i-1} \frac{\partial l_j}{\partial x}, \quad \forall i \in \{1, \dots, N\}. \quad (4)$$

We call these functions edge functions or histopolation functions associated with the Lagrange functions  $\{l_i\}_{i=0}^N$ , using the terminology of Gerritsma [16]. It is straightforward to check that the histopolation property

$$\int_{x_{i-1}}^{x_i} h_j(x) \, dx = \delta_{i,j}, \quad \forall i, j \in \{1, \dots, N\}, \quad (5)$$

holds. This property is analogous to the Lagrange property on the grid nodes but instead applies to the integrals over the sub-intervals defined by these nodes. It follows that  $\{h_i\}_{i=0}^N$  are linearly independent functions and the span of these functions is a space of dimension  $N$ . Since the  $h_i$  are sums of derivatives of the Lagrange functions, we know that  $h_i \in U_h$  for all  $i \in \{1, \dots, N\}$ . On the other hand, the dimension of  $U_l$  is  $N+1$  and  $U_l$  contains all constant functions. Hence,  $\dim(U_h) = \dim\left(\frac{\partial}{\partial x}(U_l)\right) = N$ , which shows that  $U_h$  is the span of the histopolation functions. In addition, we know that all constant functions are contained in  $U_h$  since the linear functions are contained in  $U_l$ . This is equivalent to

$$\sum_{i=1}^N (x_{i+1} - x_i) h_i(x) = 1, \quad \forall x \in [a, b]. \quad (6)$$

Given a function  $g \in U_h$ , the histopolation property (5) of the edge functions implies that the functions  $h_i$  form a complete basis for  $U_h$ , i.e.

$$g(x) = \sum_{i=1}^N \left( \int_{x_{i-1}}^{x_i} g(s) \, ds \right) h_i(x) =: \sum_{i=1}^N \bar{g}_i h_i(x). \quad (7)$$

Let the interpolation operator  $p^1$  and the histopolation operator  $p^0$  be defined as

$$p^0(f) := \sum_{i=0}^N f_i l_i = \sum_{i=0}^N f(x_i) l_i, \quad f \in C^1(I), \quad (8)$$

$$p^1(g) := \sum_{i=1}^N \bar{g}_i h_i = \sum_{i=1}^N \left( \int_{x_{i-1}}^{x_i} g(s) \, ds \right) h_i, \quad g \in C^0(I), \quad (9)$$

then we obtain the key relationship

$$\frac{\partial}{\partial x} p^0(f) = p^1 \left( \frac{\partial}{\partial x} f \right), \quad \forall f \in C^1(I). \quad (10)$$

We also have for a function  $f$  that

$$\int_{x_{i-1}}^{x_i} \frac{\partial f}{\partial x}(x) \, dx = f(x_i) - f(x_{i-1}), \quad \forall i \in \{1, \dots, N\}, \quad (11)$$

and using Eq. (4), we obtain

$$p^1 \left( \frac{\partial}{\partial x} f \right) = \sum_{j=1}^N (f_j - f_{j-1}) h_j = \frac{\partial}{\partial x} \left( \sum_{i=0}^N f_i l_i \right) = \frac{\partial}{\partial x} p^0(f). \quad (12)$$

If we have the derivative values of the  $l_i$  functions on our grid points, we can define the derivative matrix  $\underline{D} = (D_{i,j})_{i,j=0}^N$  with entries

$$D_{i,j} = \frac{\partial l_j}{\partial x}(x_i), \quad \forall i, j \in \{0, \dots, N\}, \quad (13)$$

which acts as a discrete derivative operator

$$\underline{f}' = \underline{D} \underline{f}, \quad (14)$$

where  $\underline{f}'$  contains the nodal values of the approximate derivative of the function  $f$ .

It is important to note that the nodal derivative matrix  $\underline{D}$  allows us to directly compute the histopolation basis  $h_i$  at the grid points using (4), defining the histopolation Vandermonde matrix  $\underline{V}$ :

$$V_{k,i} := h_i(x_k) = - \sum_{j=0}^{i-1} D_{k,j}, \quad \forall i \in \{1, \dots, N\}, k \in \{0, \dots, N\}. \quad (15)$$

**Remark 1.** For SBP-FD schemes, typically no continuous basis functions  $l_i$  and/or  $h_i$  are known. Only the value of the functions and their derivatives are known at the grid nodes. Hence, the relation Eq. (15) is a key observation that we use to construct discrete mimetic FD operators.

Returning to the key relation Eq. (10) evaluated at a fixed grid point  $x_i$ , as  $\sum_{k=0}^N D_{i,k} = 0$ , we obtain directly

$$\begin{aligned} \frac{\partial}{\partial x} p_0(f)(x_i) &= \sum_{k=0}^N D_{i,k} f_k &= (\underline{D}\underline{f})_i \\ &= - \sum_{j=1}^N \left( (f_j - f_{j-1}) \sum_{k=0}^{j-1} D_{i,k} \right) &= (\underline{V} \underline{\Delta} \underline{f})_i = p_1 \left( \frac{\partial}{\partial x} f \right) (x_i) \end{aligned}$$

with  $\underline{\Delta} = (\Delta_{i,j})_{i=1,j=0}^N$ ,

$$\underline{\Delta} = \begin{pmatrix} -1 & 1 & 0 & 0 & \dots \\ 0 & -1 & 1 & 0 & \dots \\ 0 & 0 & -1 & 1 & \dots \\ \vdots & \vdots & \vdots & \vdots & \ddots \end{pmatrix} \quad (16)$$

This difference matrix is a derivative matrix from the coefficients in the Lagrange basis to the coefficients in the histopolation basis encoding the derivative formula (12). Indeed, for a coefficient vector  $\underline{f} := (f_0, \dots, f_N)^T$  of a function  $f \in U_l$  in the Lagrange basis we obtain

$$\underline{\Delta} \underline{f} = (f_1 - f_0, \dots, f_N - f_{N-1})^T, \quad (17)$$

where  $(f_1 - f_0, \dots, f_N - f_{N-1})^T$  is the coefficient vector of the derivative of  $f$  in the histopolation basis. The difference matrix together with reduction operators

$R^0$  and  $R^1$ ,

$$R^0 : U_l \longrightarrow \mathbb{R}^{N+1}; \quad \sum_{i=0}^N f_i l_i(x) \longmapsto (f_0, \dots, f_N)^T, \quad (18)$$

$$R^1 : U_h \longrightarrow \mathbb{R}^N; \quad \sum_{i=1}^N \bar{g}_i h_i(x) \longmapsto (\bar{g}_1, \dots, \bar{g}_N)^T, \quad (19)$$

and the derivative formula (12), form the commuting diagram of Fig. 1, which is the discrete de Rham complex in 1D. We further have the important identity

$$\underline{D} = \underline{V} \underline{\Delta}, \quad (20)$$

which relates the nodal derivative matrix  $\underline{D}$  with the histopolation Vandermonde matrix  $\underline{V}$  and the difference matrix  $\underline{\Delta}$ . This identity further relates the Lagrange coefficients to the histopolation coefficients of the derivative. We can now use these representations of the derivative to describe derivative operators in higher dimensions.

## 2.2. Derivative Operators

The main idea of what follows is motivated by the work of Gerritsma [16], and Gerritsma et al. [17] which we aim to combine with our findings on the discrete relationships of  $\underline{D}$ ,  $\underline{V}$ , and  $\underline{\Delta}$  for general Lagrange and histopolation basis functions, which do not have to be polynomials. In particular, we are interested in high-order SBP-FD operators, for which we know the basis function values and their derivatives at the grid points. In the following, vector-valued derivative operators will be denoted by bold fonts.

To represent a function  $\phi$  in 3D, we use a tensor product ansatz, using the space  $U_l \otimes U_l \otimes U_l$ ,

$$\phi(x, y, z) = \sum_{i=0}^N \sum_{j=0}^N \sum_{k=0}^N \phi_{i,j,k} l_i(x) l_j(y) l_k(z). \quad (21)$$

Considering partial derivatives of  $\phi$ , we obtain, for instance, for the derivative in the  $x$ -direction

$$\frac{\partial}{\partial x} \phi(x, y, z) = \sum_{i=1}^N \sum_{j=0}^N \sum_{k=0}^N (\phi_{i,j,k} - \phi_{i-1,j,k}) h_i(x) l_j(y) l_k(z). \quad (22)$$

with the other derivatives evaluated analogously.

As described in [16], the histopolation derivative (22) can be used directly to define a discrete **grad** operator from the space  $(U_l \otimes U_l \otimes U_l)^T$  to the space  $(U_h \otimes U_l \otimes U_l, U_l \otimes U_h \otimes U_l, U_l \otimes U_l \otimes U_h)$ . The approximation spaces for the **curl** and **div** operators are adjusted accordingly with tensor product combinations of Lagrange and histopolation functions, where the general rule is that

the directions in which derivatives are applied are represented by  $U_l$  and other directions are represented by  $U_h$ . For a more detailed explanation, see [17].

As mentioned, our goal is to obtain purely discrete versions of these approximations at grid nodes for our mimetic FD approximations. It is straight forward to use the relationships in section 2.1 to obtain analogous expressions for **grad**, **curl**, and **div** that are purely nodal-based. We do note however, that the underlying degrees of freedom are in general not only nodal, but also consist of line, area and volume integral degrees of freedom of the cell complex induced by the tensor product grid. The derivative matrix however gives us a way of computing nodal values from the integral degrees of freedom.

For instance, the partial derivative in  $x$ -direction of the function  $\phi$  evaluated at the grid points can be computed as

$$\frac{\partial}{\partial x} \phi(x_i, y_j, z_k) = \sum_{s=1}^N V_{i,s} (\phi_{s,j,k} - \phi_{s-1,j,k}) = \sum_{s=0}^N D_{i,j} \phi_{s,j,k}. \quad (23)$$

Note that we can compute these operators without knowing the underlying basis functions.

In the following, we present discrete versions of all operators described by Gerritsma [16], which can be computed using arbitrary Lagrange and histopolation basis functions, for which we only need to know the function values and their derivatives at the grid nodes. On the other hand, as long as the values of the basis functions at the grid nodes are known, we can build the operators without having access to explicit basis functions. For instance, we can use high-order SBP-FD operators.

### 2.2.1. Gradient Operator

Assume the function  $\phi$  from the tensor product space  $U_l \otimes U_l \otimes U_l$  given through the nodal grid values  $\{\phi_{i,j,k}\}_{i,j,k=0}^N$ . Let  $\mathbf{grad}(\phi) = \mathbf{u} = (u^x, u^y, u^z)^T$ , where  $u^x \in U_h \otimes U_l \otimes U_l$ ,  $u^y \in U_l \otimes U_h \otimes U_l$ , and  $u^z \in U_l \otimes U_l \otimes U_h$ . Then the nodal values of the components of  $\mathbf{u}$  are

$$u^x(x_i, y_j, z_k) = \sum_{s=1}^N V_{i,s} (\phi_{s,j,k} - \phi_{s-1,j,k}) = \sum_{s=0}^N D_{i,j} \phi_{s,j,k}, \quad (24)$$

$$u^y(x_i, y_j, z_k) = \sum_{s=1}^N V_{i,s} (\phi_{i,s,k} - \phi_{i,s-1,k}) = \sum_{s=0}^N D_{j,s} \phi_{i,s,k}, \quad (25)$$

$$u^z(x_i, y_j, z_k) = \sum_{s=1}^N V_{i,s} (\phi_{i,j,s} - \phi_{i,j,s-1}) = \sum_{s=0}^N D_{k,s} \phi_{i,j,s}. \quad (26)$$

### 2.2.2. Curl Operator

We aim to define the **curl** operator in a space compatible with the gradient operator described above, so that we preserve the well-known identity that the curl of the gradient of a scalar field is zero. We choose  $\tilde{\mathbf{u}} = (\tilde{u}^x, \tilde{u}^y, \tilde{u}^z)$  from the same space as  $\mathbf{grad}(\phi)$  defined above. I.e., we have  $\tilde{u}^x$  is from the tensor

product space  $U_h \otimes U_l \otimes U_l$ ,  $\tilde{u}^y$  from  $U_l \otimes U_h \otimes U_l$ , and  $\tilde{u}^z$  from  $U_l \otimes U_l \otimes U_h$ . Then the nodal values of  $\mathbf{curl}(\tilde{\mathbf{u}}) = \mathbf{w} = (w^x, w^y, w^z)^T$  are given by

$$\begin{aligned} w^x(x_i, y_j, z_k) &= \sum_{s=1}^N \sum_{t=1}^N (\tilde{u}_{i,s,t}^z - \tilde{u}_{i,s-1,t}^z - \tilde{u}_{i,s,t}^y + \tilde{u}_{i,s,t-1}^y) V_{j,s} V_{k,t} \\ &= \sum_{s=1}^N \sum_{t=1}^N \tilde{u}_{i,s,t}^z D_{j,s} V_{k,t} - \tilde{u}_{i,s,t}^y V_{j,s} D_{k,t}, \end{aligned} \quad (27)$$

$$\begin{aligned} w^y(x_i, y_j, z_k) &= \sum_{s=1}^N \sum_{t=1}^N (\tilde{u}_{s,j,t}^x - \tilde{u}_{s,j,t-1}^x - \tilde{u}_{s,j,t}^z + \tilde{u}_{s-1,j,t}^z) V_{i,s} V_{k,t} \\ &= \sum_{s=1}^N \sum_{t=1}^N \tilde{u}_{s,j,t}^x V_{i,s} D_{k,t} - \tilde{u}_{s,j,t}^z D_{i,s} V_{k,t}, \end{aligned} \quad (28)$$

$$\begin{aligned} w^z(x_i, y_j, z_k) &= \sum_{s=1}^N \sum_{t=1}^N (\tilde{u}_{s,t,k}^y - \tilde{u}_{s-1,t,k}^y - \tilde{u}_{s,t,k}^x + \tilde{u}_{s,t-1,k}^x) V_{i,s} V_{j,t} \\ &= \sum_{s=1}^N \sum_{t=1}^N \tilde{u}_{s,t,k}^y D_{i,s} V_{j,t} - \tilde{u}_{s,t,k}^x V_{i,s} D_{j,t}. \end{aligned} \quad (29)$$

If  $\tilde{\mathbf{u}}$  is indeed computed as the gradient of a scalar field, we can insert the coefficients from the gradient operator in Eqs. (24),(25) and (26) for the coefficients of  $\tilde{\mathbf{u}}$ . We obtain for the coefficient of the first component of the curl

$$\begin{aligned} &u_{i,j}^k - u_{i,j-1}^k - u_{i,k}^j + u_{i,k-1}^j \\ &= \phi_{i,j,k} - \phi_{i,j,k-1} - \phi_{i,j-1,k} + \phi_{i,j-1,k-1} \\ &\quad - \phi_{i,j,k} + \phi_{i,j-1,k} + \phi_{i,j,k-1} - \phi_{i,j-1,k-1} \\ &= 0, \end{aligned} \quad (30)$$

for all indices  $i \in \{0, \dots, N\}$  and  $j, k \in \{1, \dots, N\}$ . Analogously the coefficients cancel out to zero for the other two components of the curl.

As a consequence we have for our discrete FD operators

$$\mathbf{curl}(\mathbf{u}) = \mathbf{curl}(\mathbf{grad}(\phi)) = \mathbf{0}, \quad (31)$$

or, respectively

$$\mathbf{curl} \circ \mathbf{grad} = \mathbf{0}. \quad (32)$$

### 2.2.3. Divergence Operator

Again, we want to calculate div in a space that is compatible with the above **curl** operator, so that we preserve the well-known identity that the divergence of the curl of a vector field is zero. We choose  $\tilde{\mathbf{w}} = (\tilde{w}^x, \tilde{w}^y, \tilde{w}^z)$  from the same space as  $\mathbf{curl}(\tilde{\mathbf{u}})$  defined above. I.e.,  $\tilde{w}^x$  is from the tensor product space  $U_l \otimes U_h \otimes U_h$ ,  $\tilde{w}^y$  from  $U_h \otimes U_l \otimes U_h$ , and  $\tilde{w}^z$  from  $U_h \otimes U_h \otimes U_l$ . Then the nodal

$$H^1 \xrightarrow{\text{curl}} H(\text{div}) \xrightarrow{\text{div}} L^2$$

Figure 2: 2D de Rham complex

$$L^2 \xleftarrow{\text{curl}} H(\text{curl}) \xleftarrow{\text{-grad}} H^1$$

Figure 3: 2D dual de Rham complex

values of  $\text{div}(\tilde{\mathbf{w}}) = f$  are given by

$$\begin{aligned} f(x_i, y_j, z_z) &= \sum_{s=1}^N \sum_{t=1}^N \sum_{r=1}^N (\tilde{w}_{s,t,r}^x - \tilde{w}_{s-1,t,r}^x + \tilde{w}_{s,t,r}^y \\ &\quad - \tilde{w}_{s,t-1,r}^y + \tilde{w}_{s,t,r}^z - \tilde{w}_{s,t,r-1}^z) V_{i,s} V_{j,t} V_{k,r} \\ &= \sum_{s=1}^N \sum_{t=1}^N \sum_{r=1}^N \tilde{w}_{s,t,r}^x D_{i,s} V_{j,t} V_{k,r} \\ &\quad + \tilde{w}_{s,t,r}^y V_{i,s} D_{j,t} V_{k,r} + \tilde{w}_{s,t,r}^z V_{i,s} V_{j,t} D_{k,r}. \end{aligned} \quad (33)$$

Analogously to the **curl** operator, we can insert the coefficients of the curl into the divergence operator to obtain

$$\text{div}(\mathbf{w}) = \text{div}(\text{curl}(\tilde{\mathbf{u}})) = \mathbf{0}, \quad (34)$$

or, respectively

$$\text{div} \circ \text{curl} = \mathbf{0}. \quad (35)$$

#### 2.2.4. 2D Operators

In 2D, we have four relevant derivative operators on our discrete spaces that we can use to find a discrete counterpart to the 2D primal and dual de Rham complexes of Fig. 2 and Fig. 3. The 2D **grad** and **div** operators, one scalar-to-vector  $\text{curl} = \left( \frac{\partial}{\partial y}, -\frac{\partial}{\partial x} \right)^T$  and a vector-to-scalar  $\text{curl} \left( (v^x, v^y)^T \right) = \frac{\partial v^y}{\partial x} - \frac{\partial v^x}{\partial y}$ . Both **grad** and **curl** are defined for functions  $u \in U_l \otimes U_l$  while **div** is defined for functions  $\mathbf{v} \in (U_l \otimes U_h, U_h \otimes U_l)^T$ . Finally, the **curl** operator is defined for functions  $\mathbf{w} \in (U_h \otimes U_l, U_l \otimes U_h)^T$ .

In all cases, we have Lagrange basis functions in the directions in which we take the derivatives and histopolation functions otherwise. In the following, we will write the degrees of freedom for all functions in vector form, where we save them in the following order:

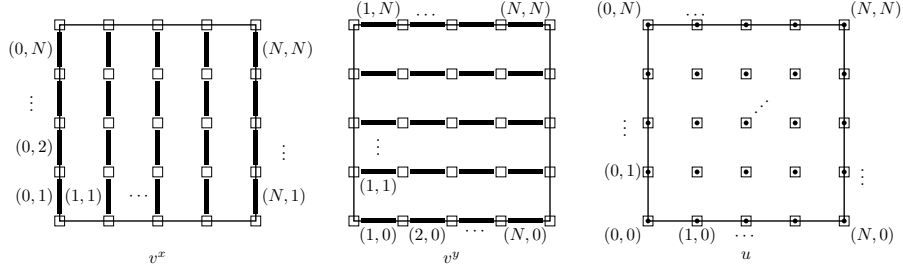


Figure 4: Storage of the degrees of freedom for 2D functions

$$\mathbf{v}^x = \begin{bmatrix} v_{01}^x \\ \vdots \\ v_{N1}^x \\ v_{02}^x \\ \vdots \\ v_{N2}^x \\ \vdots \\ v_{NN}^x \end{bmatrix} \in \mathbb{R}^{N(N+1)}, \quad \mathbf{v}^y = \begin{bmatrix} v_{10}^y \\ \vdots \\ v_{N0}^y \\ v_{11}^y \\ \vdots \\ v_{N1}^y \\ \vdots \\ v_{NN}^y \end{bmatrix} \in \mathbb{R}^{N(N+1)}, \quad (36)$$

$$\mathbf{u} = \begin{bmatrix} u_{00} \\ \vdots \\ u_{N0} \\ u_{01} \\ \vdots \\ u_{N1} \\ \vdots \\ u_{NN} \end{bmatrix} \in \mathbb{R}^{(N+1)^2}, \quad (37)$$

where  $\mathbf{v}$  is a function for which we require to compute its gradient. Analogously to  $\mathbf{u}$ , we can define the discrete storage of a function  $\mathbf{w}$ , for which we need to compute its **curl**. Using the Kronecker product, we can define the 2D partial derivative operators in matrix form:

$$\underline{\Delta}_x^{2D} := \underline{I}_{N+1} \otimes \underline{\Delta} \in \mathbb{R}^{N(N+1) \times (N+1)^2}, \quad (38)$$

$$\underline{\Delta}_y^{2D} := \underline{\Delta} \otimes \underline{I}_{N+1} \in \mathbb{R}^{N(N+1) \times (N+1)^2}, \quad (39)$$

where  $\underline{I}_{N+1}$  is the identity matrix of the corresponding dimension.

$$\begin{array}{ccccccc}
H^1 & \xrightarrow{\text{curl}} & H(\text{div}) & \xrightarrow{\text{div}} & L^2 & & \\
\downarrow p^0 & & \downarrow \mathbf{p}^1 & & \downarrow p^2 & & \\
W^0 & \xrightarrow{\text{curl}} & W^1 & \xrightarrow{\text{div}} & W^2 & & \\
\downarrow R^0 & & \downarrow \mathbf{R}^1 & & \downarrow R^2 & & \\
\mathbb{R}^{(N+1)^2} & \xrightarrow{\text{curl}} & \mathbb{R}^{(N+1)N} \times \mathbb{R}^{N(N+1)} & \xrightarrow{\text{div}} & \mathbb{R}^{N^2} & & 
\end{array}$$

Figure 5: Discrete dual de Rham complex in 2D

Now we can write the derivative operators in matrix form:

$$\underline{\text{grad}}^x(\mathbf{u}) = \underline{\Delta}_x^{2D} \mathbf{u}, \quad (40)$$

$$\underline{\text{grad}}^y(\mathbf{u}) = \underline{\Delta}_y^{2D} \mathbf{u}, \quad (41)$$

$$\underline{\text{curl}}^x(\mathbf{u}) = \underline{\Delta}_y^{2D} \mathbf{u}, \quad (42)$$

$$\underline{\text{curl}}^y(\mathbf{u}) = -\underline{\Delta}_x^{2D} \mathbf{u}, \quad (43)$$

$$\underline{\text{curl}}(\mathbf{w}^x, \mathbf{w}^y) = \underline{\Delta}_x^{2D} \mathbf{w}^y - \underline{\Delta}_y^{2D} \mathbf{w}^x, \quad (44)$$

$$\underline{\text{div}}(\mathbf{v}^x, \mathbf{v}^y) = \underline{\Delta}_x^{2D} \mathbf{v}^x + \underline{\Delta}_y^{2D} \mathbf{v}^y, \quad (45)$$

and we obtain

$$\underline{\text{curl}} \circ \underline{\text{grad}}(\mathbf{u}) = (\underline{\Delta}_y^{2D} \underline{\Delta}_x^{2D} - \underline{\Delta}_x^{2D} \underline{\Delta}_y^{2D}) \mathbf{u} = \underline{0}, \quad (46)$$

$$\underline{\text{div}} \circ \underline{\text{curl}}(\mathbf{u}) = (\underline{\Delta}_x^{2D} \underline{\Delta}_y^{2D} - \underline{\Delta}_y^{2D} \underline{\Delta}_x^{2D}) \mathbf{u} = \underline{0}, \quad (47)$$

where we have used the following property of Kronecker products:

$$(\underline{A} \otimes \underline{B})(\underline{C} \otimes \underline{D}) = \underline{AC} \otimes \underline{BD}. \quad (48)$$

With the matrix representation of our derivative operators, we have the commuting 2D dual de Rham complex of Fig. 5, using reduction operators  $R^0, \mathbf{R}^1$  and  $R^2$ . These operators are defined as the mappings sending functions in the discrete spaces to the vector of their degrees of freedom. We can again evaluate the operators nodally using the histopolation Vandermonde matrix  $\underline{V}$  analogously to the 3D case in equations (24) to (33).

### 2.3. Summation-By-Parts Finite Difference Operators

In the previous section, we assumed the existence of Lagrange functions that fulfill (2) and (3) at grid points  $\{x_i\}_{i=0}^N$  (including the boundary nodes), but we did not discuss how to construct them. In [17], Gerritsma uses the Legendre–Gauss–Lobatto points and the Lagrange interpolating polynomials for those points. The corresponding derivative matrix  $\underline{D}$  together with the mass matrix

$\underline{M}$ , which is a diagonal matrix with the Legendre–Gauss–Lobatto quadrature weights on the diagonal, has the summation-by-parts (SBP) property,

$$\underline{M}\underline{D} + \underline{D}^T \underline{M} = \underline{B}, \quad (49)$$

where

$$B_{i,j} = -\delta_{0,i}\delta_{0,j} + \delta_{N,i}\delta_{N,j} \quad (50)$$

is a boundary matrix.

As we have pointed out above, we only need to evaluate our basis functions and their derivatives at the grid nodes to construct the mimetic operators defined in the previous section. If we use a collocation quadrature rule when applying Finite Element Exterior Calculus [1, 2] to derive our scheme, the global shape of the basis functions  $l_i$  does not matter at all, only their nodal function and derivative values are relevant. The central idea of this paper is therefore to not construct basis functions  $l_i$  at all, but use existing diagonal norm finite difference SBP operators, for example from Strand [26], to supply a quadrature rule and nodal derivative data needed for the numerical scheme. We do this explicitly by prescribing the nodal derivatives of the Lagrange functions, that are not known globally, through the derivative matrix according to (13) and using diagonal entries of the norm matrix  $\underline{M}$  as weights for a collocation quadrature rule on the grid points.

One of the standard SBP finite difference operators from [26], which we will use in this study, is the operator with interior order 4 and boundary order 2 with  $N + 1$  points:

$$\underline{D} = \frac{1}{\Delta x} \begin{pmatrix} -\frac{24}{17} & \frac{59}{34} & \frac{4}{17} & -\frac{3}{34} & 0 & 0 & 0 & \dots \\ -\frac{1}{2} & 0 & \frac{1}{2} & 0 & 0 & 0 & 0 & \dots \\ \frac{4}{2} & -\frac{59}{86} & 0 & \frac{59}{86} & -\frac{4}{43} & 0 & 0 & \dots \\ \frac{43}{98} & 0 & -\frac{59}{98} & 0 & \frac{32}{49} & -\frac{4}{49} & 0 & \dots \\ 0 & 0 & \frac{1}{12} & -\frac{2}{3} & 0 & \frac{2}{3} & -\frac{1}{12} & \dots \\ & & & & & & & \dots \end{pmatrix}, \quad (51)$$

$$\underline{M} = \Delta x \operatorname{diag} \left( \frac{17}{48}, \frac{59}{48}, \frac{43}{48}, \frac{49}{48}, 1, \dots, 1, \frac{49}{48}, \frac{43}{48}, \frac{59}{48}, \frac{17}{48} \right), \quad (52)$$

which is defined on an equidistant grid, where  $\Delta x$  is the distance between two neighboring grid nodes. In the derivative matrix, the upper right boundary block is repeated in the bottom left with reversed signs and inverted order.

In the following, we will derive a mimetic scheme for the 2D transverse electric Maxwell's equations to validate our approach.

### 3. Mimetic Scheme for the 2D Maxwell's Equations

#### 3.1. Maxwell's Equations in 2D

The homogeneous transverse electric Maxwell's equations with unit light speed read

$$\frac{\partial B^z}{\partial t} + \text{curl}(\mathbf{E}) = 0, \quad (53)$$

$$\frac{\partial \mathbf{E}}{\partial t} - \text{curl}(B^z) = \mathbf{0}, \quad (54)$$

$$\text{div}(\mathbf{E}) = 0. \quad (55)$$

Our goal is to derive a mimetic scheme using finite element exterior calculus to preserve the divergence involution (55). For simplicity we will consider a periodic and rectangular domain, using a Cartesian mesh for the discretization. To apply the framework of Finite Element Exterior Calculus, we need the de Rham complexes containing the derivative operators of the PDEs.

#### 3.2. De Rham Complexes

The Maxwell's equations have an inherent geometric structure described by the de Rham cochain complex of Fig. 2 and its dual in Fig. 3 in 2D. We define the spaces needed for the complexes by

$$H(\text{curl}) = \{\mathbf{w} \in L^2 \mid \text{curl}(\mathbf{w}) \in L^2\}, \quad (56)$$

$$H(\text{div}) = \{\mathbf{w} \in L^2 \mid \text{div}(\mathbf{w}) \in L^2\}. \quad (57)$$

The complexes are dual in the sense that

$$\langle \text{curl}(\psi), \Phi \rangle = \langle \psi, \text{curl}(\Phi) \rangle, \quad \forall \psi \in H^1, \Phi \in H(\text{curl}), \quad (58)$$

$$\langle \text{div}(\Psi), \phi \rangle = \langle \Psi, -\text{grad}(\phi) \rangle, \quad \forall \Psi \in H(\text{div}), \phi \in H^1, \quad (59)$$

where the brackets denote the  $L^2$  inner product. These equations only hold in the periodic case. In the non-periodic case the boundary integral does not vanish by default, which means we would have to restrict the spaces of one of the two complexes to restore duality.

In Maxwell's equation we use operators from both complexes, so we have to choose in which spaces to look for  $\mathbf{E}$  and  $B^z$ . If we choose  $\mathbf{E} \in H(\text{div})$  and  $B^z \in H^1$ , we can solve Ampère's law and Gauss's law strongly, while we have to use Stokes' theorem to solve Faraday's law weakly, while for  $\mathbf{E} \in H(\text{curl})$  and  $B^z \in L^2$ , we can solve Faraday's law strongly, but need to solve Ampère's law and Gauss's law weakly.

Since the divergence involution for the magnetic field falls away in the 2D transverse electric case and we want to preserve Gauss' law for the electric field (55),

we will choose  $\mathbf{E} \in H(\text{div})$  and  $B^z \in H^1$ , leading to the formulation:

$$\left\langle \frac{\partial B^z}{\partial t}, \psi \right\rangle + \langle \mathbf{E}, \mathbf{curl}(\psi) \rangle = 0, \quad \forall \psi \in H^1, \quad (60)$$

$$\left\langle \frac{\partial \mathbf{E}}{\partial t}, \Phi \right\rangle + \langle \mathbf{curl}(B^z), \Phi \rangle = 0, \quad \forall \Phi \in H(\text{div}), \quad (61)$$

$$\langle \text{div}(\mathbf{E}), \mu \rangle = 0, \quad \forall \mu \in L^2. \quad (62)$$

The finite element exterior calculus ansatz is to choose a discrete subcomplex of the de Rham complex, meaning we choose  $W^0 \subset H^1$ ,  $W^1 \subset H(\text{curl})$ ,  $W^2 \subset L^2$  such that  $\mathbf{curl}(W^0) \subset W^1$  and  $\text{div}(W^1) \subset W^2$ . In addition we need bounded projections  $p_0, \mathbf{p}_1$  and  $p_2$ , so that the diagram of Fig. 5 commutes.

We then restrict both our ansatz and our test spaces to the corresponding finite dimensional subspaces. This means we again have two ansatz spaces for the electric and magnetic field: We look for a numerical solution  $\mathbf{E} \in [0, T] \times W^1$  and  $B^z \in [0, T] \times W^2$  so that

$$\left\langle \frac{\partial B^z}{\partial t}, \psi \right\rangle + \langle \mathbf{E}, \mathbf{curl}(\psi) \rangle = 0, \quad \forall \psi \in W^2, \quad (63)$$

$$\left\langle \frac{\partial \mathbf{E}}{\partial t}, \Phi \right\rangle + \langle \mathbf{curl}(B^z), \Phi \rangle = 0, \quad \forall \Phi \in W^1, \quad (64)$$

$$\langle \text{div}(\mathbf{E}), \mu \rangle = 0, \quad \forall \mu \in W^0. \quad (65)$$

Since  $\text{div}(\mathbf{E}) \in W^0$  we do get  $\text{div}(\mathbf{E}) \equiv 0$  from (65). We will later show that by solving (63) and (64) with this method, we automatically preserve the divergence involution both in the semi-discrete and fully discrete setting. Therefore we will only consider the evolution equations (63) and (64) when deriving our method.

### 3.3. Spaces and Projections

To construct our spaces and projections, we first look at the one-dimensional case. We have a one-dimensional periodic domain  $\Omega$  and a partition of  $\{E^k\}_{k=1}^m$  of  $\Omega$  into elements. We further assume that we have a Lagrange basis  $\{\tilde{l}_i^k\}_{i=0}^N$  as specified in 2.1 for each element  $E^k$ , that we can get as a linear transformation of such a basis from a reference element. We further have the derived histoppolation functions  $\{\tilde{h}_i^k\}_{i=1}^N$ . Now, we can construct spaces basis functions  $\{l_i^k\}_{i=0, k=1}^{N-1, m}$  and

$\{h_i^k\}_{i,k=1}^{N,m}$  that are defined on the whole domain as follows for all  $k \in \{1, \dots, m\}$ :

$$l_i^k(x) := \begin{cases} \tilde{l}_i^k(x) & \text{for } x \in E^k, \\ 0 & \text{for } x \in E^l, l \neq k, \end{cases} \quad \forall i \in \{1, \dots, N-1\}, \quad (66)$$

$$l_0^k(x) := \begin{cases} \tilde{l}_0^k(x) & \text{for } x \in E^k, \\ \tilde{l}_N^{\sigma(k)}(x) & \text{for } x \in E^{\sigma(k)}, \\ 0, & \text{for } x \in E^l, l \neq k, l \neq \sigma(k) \end{cases} \quad (67)$$

$$l_N^k(x) := \begin{cases} \tilde{l}_N^k(x) & \text{for } x \in E^k, \\ \tilde{l}_0^{\sigma(k)}(x) & \text{for } x \in E^{\sigma(k)}, \\ 0 & \text{for } x \in E^l, l \neq k, l \neq \sigma(k), \end{cases} \quad (68)$$

$$h_i^k(x) := \begin{cases} \tilde{h}_i^k(x) & \text{for } x \in E^k, \\ 0 & \text{for } x \in E^l, l \neq k, \end{cases} \quad \forall i \in \{1, \dots, N\}, \quad (69)$$

where  $\sigma(k)$  is defined as the element index of the right neighbor of the element with index  $k$  and  $\tilde{\sigma}(k)$  is the index of the left neighbor of element  $k$ . Here  $l_N^k$  and  $l_0^{\sigma(k)}$  refer to the same function, as do  $l_0^k$  and  $l_N^{\tilde{\sigma}(k)}$ . While the Lagrange basis is globally continuous, the histopolation basis does not have a unique value at element boundaries. When we use the nodal evaluation matrix for the histopolation functions (15), we will do so for each element separately and obtain the value of the continuous extension of the basis functions to the boundary when restricted to the element in question.

Analogously to 2.1 we can now define the space  $U_l$  as the span of the global Lagrange functions and  $U_h$  as the span of the global histopolation functions. We again have  $\frac{\partial}{\partial x}(U_l) = U_h$ , where  $\frac{\partial}{\partial x}$  is the weak derivative operator, even though we have in the periodic case the same number of degrees of freedom. This is because there is an additional continuity requirement at the domain boundary that breaks down when taking the derivative. Now, in analogy to (8) and (9), let  $p^0$  be the global histopolation operator and  $p^1$  the global interpolation operator associates with the defined bases.

We can apply the derivative formula (12) element-wise to obtain the commutation property (10) for the multi-element case. This means the commuting diagram 1 for the one-dimensional de Rham complex commutes. To extend this approach to 2D, we use a tensor product ansatz, where for a rectangular periodic domain  $\Omega$  with a Cartesian grid, we define the discrete spaces via a tensor product ansatz as follows:

$$W^0 := U_h \otimes U_h, \quad (70)$$

$$W^1 := (U_l \otimes U_h, U_h \otimes U_l)^T, \quad (71)$$

$$W^2 := U_l \otimes U_l. \quad (72)$$

Here we have a slight abuse of notation because we can have different number of elements and scaling factors in both directions. The projections  $p_0, p_1$ , and

$p_2$  are now defined by taking the interpolation in the directions where we use the space  $U_l$  and histopolation in the directions where we have  $U_h$ :

$$p^0(f) := \sum_{k=1}^m \sum_{i,j=1}^N \sum_{k=1}^m \sum_{i,j=1}^N \left( \int_{x_{i-1}^k}^{x_i^k} \int_{y_{j-1}^k}^{y_j^k} f(s, t) \, ds \, dt \right) h_i^k(x) h_j^k(y), \quad (73)$$

$$p_1^1(\mathbf{f}) := \sum_{k=1}^m \sum_{i=0}^{N-1} \sum_{j=1}^N \left( \int_{y_{j-1}^k}^{y_j^k} f(x_i^k, t) \, dt \right) l_i^k(x) h_j^k(y), \quad (74)$$

$$p_2^1(\mathbf{f}) := \sum_{k=1}^m \sum_{i=1}^N \sum_{j=0}^{N-1} \left( \int_{x_{i-1}^k}^{x_i^k} f(s, y_j^k) \, ds \right) h_i^k(x) l_j^k(y), \quad (75)$$

$$p^2(f) := \sum_{k=1}^m \sum_{i,j=0}^{N-1} f(x_i^k, y_j^k) l_i(x) l_j(y). \quad (76)$$

Since we use the same DOFs as Gerritsma et al. [17], the boundedness of the projections carries over, since we can factorize over Gerritsma's projections switching out the basis functions. As a linear mapping between finite dimensional vector spaces, it is bounded, and therefore our projections are bounded as the composition of two bounded mappings. It is straightforward to see that we also get commuting property for the discrete 2D de Rham complex 5.

## 4. Numerical Method

### 4.1. Galerkin Discretization

Before we derive the method, we have to account for the overlap in degrees of freedom associated with the basis functions associated with the boundary nodes in continuous directions. To avoid duplication that we would have to account in our formulation, we define the vectors of degrees of freedom as:

$$\underline{B}^z = \begin{pmatrix} B_{0,0;1}^z \\ \vdots \\ B_{N-1,0;1}^z \\ B_{0,1;1}^z \\ \vdots \\ B_{N-1,N-1;1}^z \\ B_{0,0;2}^z \\ \vdots \\ B_{N-1,N-1;m}^z \end{pmatrix}, \quad \underline{E}^x = \begin{pmatrix} \bar{E}_{0,1;1}^x \\ \vdots \\ \bar{E}_{N-1,1;1}^x \\ \bar{E}_{0,2;1}^x \\ \vdots \\ \bar{E}_{N-1,N;1}^x \\ \bar{E}_{0,1;2}^x \\ \vdots \\ \bar{E}_{N-1,N;m}^x \end{pmatrix}, \quad \underline{E}^y = \begin{pmatrix} \bar{E}_{1,0;1}^y \\ \vdots \\ \bar{E}_{N,0;1}^y \\ \bar{E}_{1,1;1}^y \\ \vdots \\ \bar{E}_{N,N-1;1}^y \\ \bar{E}_{1,0;2}^y \\ \vdots \\ \bar{E}_{N,N-1;m}^y \end{pmatrix}.$$

For ease of notation, we define  $B_{N,j,k} := B_{0,j,\sigma_r(k)}$ ,  $B_{i,N,k} := B_{i,0,\sigma_r(k)}$ , and  $B_{N,N,k} := B_{0,0,\sigma_r(\sigma_u(k))}$ . Here,  $\sigma_r(k)$  is defined as the index of the right neighbor element of the element  $E^k$  and  $\sigma_u(k)$  is the index of the upper neighbor of  $E^k$ .

We also apply this notation for the electric field coefficients in directions where the electric field component is continuous. Additionally, we assume for simplicity that the reference grid of our finite difference operator is of length one (which we can achieve by rescaling). Further, we assume that each element has the same length  $\Delta x$  in  $x$ - and  $\Delta y$  in  $y$ -direction. Both assumptions are not necessary, they are used to simplify the definition of our matrix operators. Since we have Lagrange functions associated with boundary nodes whose support contains two elements, we define intertwined quadrature weights

$$\tilde{\omega}_i := \begin{cases} \omega_i & \text{for } i \in \{1, \dots, N-1\}, \\ \omega_0 + \omega_N & \text{for } i = 0, i = N. \end{cases} \quad (77)$$

In addition, we require the derivative matrix  $\underline{D} \in \mathbb{R}^{N+1, N+1}$  of the finite difference operator to be of rank  $N$  and  $\underline{D}\underline{c} = 0$  for all constant vectors  $\underline{c}$ . Then  $\underline{V}$  defined by (15) has full rank and the histopolation mass matrix  $\underline{V}^T \underline{M} \underline{V}$  is symmetric positive definite and therefore invertible.

We can now derive our method via the Galerkin ansatz in (63) and (64). Using our basis functions as test functions we get for the first component of (64):

$$\begin{aligned} & \sum_{k=1}^m \sum_{i=0}^{N-1} \sum_{j=1}^N \int_{E^k} \frac{\partial}{\partial t} (E_{i,j;k}^x) l_i^k(x) h_j^k(x) l_s^l(x) h_t^l(y) \, dx \, dy \\ &= \sum_{k=1}^m \sum_{i=0}^{N-1} \sum_{j=0}^{N-1} \int_{E^k} \frac{\partial}{\partial y} (B_{i,j;k}^z l_i^k(x) h_j^k(y)) l_s^l(x) h_t^l(y) \, dx \, dy \\ &= \sum_{k=1}^m \sum_{i=0}^{N-1} \sum_{j=1}^N \int_{E^k} (B_{i,j;k}^z - B_{i,j-1;k}^z) l_i^k(x) h_j^k(y) l_s^l(x) h_t^l(y) \, dx \, dy. \end{aligned} \quad (78)$$

Using collocation with our finite difference quadrature rule on the grid leads us to

$$\begin{aligned} & \Delta x \Delta y \tilde{\omega}_s \sum_{j=1}^N \frac{\partial}{\partial t} (E_{s,j;l}^x) \sum_{o=0}^N \omega_o h_j^k(y_o^l) h_t^l(y_o^l) \\ &= \Delta x \Delta y \tilde{\omega}_s \sum_{j=1}^N (B_{s,j;l}^z - B_{s,j-1;l}^z) \sum_{o=0}^N \omega_o h_j^k(y_o^l) h_t^l(y_o^l), \end{aligned} \quad (79)$$

where the sum over the elements falls away because the support of our test functions encompasses at most two elements. We can now cancel the common factors and write it in matrix-vector form

$$\underline{V}^T \underline{M} \underline{V} \underline{E}_{s;l}^x = \underline{V}^T \underline{M} \underline{V} \underline{\Delta} B_{s;l}^z, \quad (80)$$

with  $\underline{E}_{s;l}^x := \left( \frac{\partial}{\partial t} (E_{s,1;l}^x), \dots, \frac{\partial}{\partial t} (E_{s,N;l}^x) \right)^T$  and  $\underline{B}_{s;l}^z := \left( B_{s,0;l}^x, \dots, B_{s,N;l}^x \right)^T$ . Usually the matrix  $\underline{V}$  would contain a scaling factor  $(\Delta x)^{-1}$  from the derivative

matrix, but this cancels out as well. Since the histopolation mass matrix is invertible, we obtain for all element indices  $l \in \{1, \dots, m\}$

$$\frac{\partial}{\partial t}(E_{s,j;l}^x) = B_{s,j;l}^z - B_{s,j-1;l}^z, \quad \forall s \in \{0, \dots, N\}, j \in \{1, \dots, N\}. \quad (81)$$

Analogously we obtain

$$\frac{\partial}{\partial t}(E_{i,t;l}^y) = B_{i,t;l}^z - B_{i-1,t;l}^z, \quad \forall t \in \{0, \dots, N\}, i \in \{1, \dots, N\}. \quad (82)$$

For (63) we obtain

$$\begin{aligned} & \sum_{k=1}^m \sum_{i=0}^{N-1} \sum_{j=0}^{N-1} \int_{E^k} \frac{\partial}{\partial t}(B_{i,j;k}^x) l_i^k(x) l_j^k(x) l_s^l(x) l_t^l(y) \, dx \, dy \\ &= \sum_{k=1}^m \sum_{i=0}^{N-1} \sum_{j=1}^N \int_{E^k} E_{i,j;k}^x l_i^k(x) h_j^k(y) l_s^l(x) \frac{\partial}{\partial y} l_t^l(y) \, dx \, dy \\ & \quad - \sum_{k=1}^m \sum_{i=1}^N \sum_{j=0}^{N-1} \int_{E^k} E_{i,j;k}^y h_i^k(x) l_j^k(y) \frac{\partial}{\partial x} l_s^l(x) l_t^l(y) \, dx \, dy. \end{aligned} \quad (83)$$

Using our collocation quadrature rule and canceling scaling terms we obtain for all element indices  $l \in \{1, \dots, m\}$

$$\begin{aligned} & \tilde{\omega}_s \tilde{\omega}_t \frac{\partial}{\partial t}(B_{s,t;l}^x) \\ &= \tilde{\omega}_s \sum_{j=1}^N E_{s,j;l}^x \sum_{o=0}^N \omega_o h_j^l(y_o^l) \frac{\partial}{\partial y} l_t^l(y_o^l) + T_{t;l} \quad \forall s, t \in \{0, \dots, N\}. \\ & \quad - \tilde{\omega}_t \sum_{i=1}^N E_{i,t;l}^y \sum_{o=0}^N \omega_o h_i^l(x_o^l) \frac{\partial}{\partial x} l_s^l(x_o^l) + S_{s;l}, \end{aligned} \quad (84)$$

where  $S_{s;l}$  and  $T_{t;l}$  denote terms from neighbouring elements if  $s = 0$ ,  $s = N$ ,  $t = 0$ , or  $t = N$ . For example if  $t = N$  we obtain

$$T_{t;l} = \tilde{\omega}_s \sum_{j=1}^N E_{s,j;\sigma_u(l)}^x \sum_{o=0}^N \omega_o h_j^{\sigma_u(l)}(y_o^{\sigma_u(l)}) \frac{\partial}{\partial y} l_t^l(y_o^{\sigma_u(l)}). \quad (85)$$

The other terms are analogous.

#### 4.2. Matrix-Vector Formulation

To assemble the matrix-vector form of the scheme, we need the 2D matrix operators. These we can obtain from the 1D element-wise operators via the Kronecker product. We repeat here the matrix operators from 2.1, with the special case of the derivative operators  $\Delta$  and  $\underline{D}$ . Those we have to split into two

parts because the degrees of freedoms are not duplicated in the corresponding vectors. The 1D operators also do not take into account the element size yet, this we will introduce assembling the 2D operators. For integration we obtain the regular mass matrix  $\underline{M}$  and the intertwined mass matrix  $\hat{M}$ :

$$\underline{M} = \text{diag}(\omega_0, \dots, \omega_N), \quad (86)$$

$$\hat{M} = \text{diag}(\omega_0 + \omega_N, \dots, \omega_{N-1}). \quad (87)$$

The latter results from the Lagrange functions associated with boundary nodes of an element. These have a support of two elements and are therefore integrated over both, resulting in the numerical integral  $\omega_0 + \omega_N$ . We note that this case resulting in a different mass matrix is owed to the fact that we do not save duplicated degrees of freedom. If we save all degrees of freedom of one element in one part of the overall vector and therefore include duplications in continuous directions, we could use  $\underline{M}$  in all directions.

For our derivative operators, we have  $\hat{D} \in \mathbb{R}^{N+1 \times N}$ ,  $\tilde{D} \in \mathbb{R}^{N+1 \times N}$ ,  $\underline{\Delta} \in \mathbb{R}^{N \times N}$ , and  $\hat{\Delta} \in \mathbb{R}^{N \times N}$ . Since these are element-wise operators, the derivative at the boundaries always refers to the derivative of the function restricted to the element. So the derivative at  $x_N$  would be the left-sided derivative.

$$\hat{D} := \left( \frac{\partial}{\partial x} l_j(x_i) \right)_{i=0, j=0}^{N, N-1}, \quad (88)$$

$$\tilde{D} := \begin{pmatrix} \frac{\partial}{\partial x} l_N(x_0) & 0 & \dots & 0 \\ \vdots & \dots & \vdots & \vdots \\ \frac{\partial}{\partial x} l_N(x_N) & 0 & \dots & 0 \end{pmatrix}, \quad (89)$$

$$\underline{\Delta} := (\delta_{i+1,j} - \delta_{i,j})_{i=0, j=0}^{N-1}, \quad (90)$$

$$\hat{\Delta} := (\delta_{i,N-1} \delta_{j,0})_{i=0, j=0}^{N-1}. \quad (91)$$

Furthermore, we have the Vandermonde matrix  $\underline{V} \in \mathbb{R}^{N+1 \times N}$  defined in (15). To construct the 2D operators we need the neighbour matrices  $\underline{P}^r \in \mathbb{R}^{m \times m}$  and  $\underline{P}^u \in \mathbb{R}^{m \times m}$  that encode the neighbour information as follows:

$$P_{i,j}^r := \delta_{i, \sigma_r(i)} \quad \forall i, j \in \{1, \dots, m\}, \quad (92)$$

$$P_{i,j}^u := \delta_{i, \sigma_u(i)} \quad \forall i, j \in \{1, \dots, m\}. \quad (93)$$

Let further  $\underline{I}_n \in \mathbb{R}^{n \times n}$  the identity matrix and  $\underline{A} \otimes \underline{B}$  the Kronecker product, then we can define the 2D mass matrices:

$$\hat{M}^{2D} := \Delta x \Delta y \left( \underline{I}_m \otimes \hat{M} \otimes \hat{M} \right), \quad (94)$$

$$\underline{M}_x^{2D} := \Delta x \Delta y \left( \underline{I}_m \otimes \underline{M} \otimes \hat{M} \right), \quad (95)$$

$$\underline{M}_y^{2D} := \Delta x \Delta y \left( \underline{I}_m \otimes \hat{M} \otimes \underline{M} \right), \quad (96)$$

$$\underline{M}^{2D} := \Delta x \Delta y \left( \underline{I}_m \otimes \underline{M} \otimes \underline{M} \right). \quad (97)$$

We also obtain the 2D derivative operators:

$$\underline{D}_x^{2D} := (\Delta x)^{-1} \left( \underline{I}_m \otimes \underline{I}_N \otimes \hat{D} + \underline{P}_r \otimes \underline{I}_N \otimes \tilde{D} \right), \quad (98)$$

$$\underline{D}_y^{2D} := (\Delta y)^{-1} \left( \underline{I}_m \otimes \hat{D} \otimes \underline{I}_N + \underline{P}_u \otimes \tilde{D} \otimes \underline{I}_N \right), \quad (99)$$

$$\underline{\Delta}_x^{2D} := \underline{I}_m \otimes \underline{I}_N \otimes \hat{\Delta} + \underline{P}_r \otimes \underline{I}_N \otimes \tilde{\Delta}, \quad (100)$$

$$\underline{\Delta}_y^{2D} := \underline{I}_m \otimes \hat{\Delta} \otimes \underline{I}_N + \underline{P}_u \otimes \tilde{\Delta} \otimes \underline{I}_N, \quad (101)$$

Since these operators applied to the variable vectors yield the exact derivative, we have again

$$\underline{\Delta}_x^{2D} \underline{\Delta}_y^{2D} - \underline{\Delta}_y^{2D} \underline{\Delta}_x^{2D} = 0. \quad (102)$$

The Vandermonde matrices are

$$\underline{V}_x := (\Delta x)^{-1} (\underline{I}_m \otimes \underline{I}_N \otimes \underline{V}), \quad (103)$$

$$\underline{V}_y := (\Delta y)^{-1} (\underline{I}_m \otimes \underline{V} \otimes \underline{I}_N). \quad (104)$$

We note that we again have the analogous equations to (20)

$$\underline{D}_x = \underline{V}_x^{2D} \underline{\Delta}_x^{2D}, \quad (105)$$

$$\underline{D}_y = \underline{V}_y^{2D} \underline{\Delta}_y^{2D}, \quad (106)$$

which leads to the semi-discrete scheme

$$\frac{d}{dt} \underline{\overline{E}}^x = \underline{\Delta}_y^{2D} \underline{B}^z, \quad (107)$$

$$\frac{d}{dt} \underline{\overline{E}}^y = -\underline{\Delta}_x^{2D} \underline{B}^z, \quad (108)$$

$$\hat{\underline{M}}^{2D} \frac{d}{dt} \underline{B}^z = \underline{\Delta}_x^{2D,T} \underline{V}_x^{2D,T} \underline{M}_y^{2D} \underline{V}_x^{2D} \underline{\overline{E}}^y - \underline{\Delta}_y^{2D,T} \underline{V}_y^{2D,T} \underline{M}_x^{2D} \underline{V}_y^{2D} \underline{\overline{E}}^x. \quad (109)$$

Using the Summation-by-Parts property we can also derive a strong form version of the scheme. First we rewrite the semidiscrete Faraday equation (109), using the identity  $\underline{V}\underline{\Delta} = \underline{D}$

$$\begin{aligned} \frac{d}{dt} \underline{B}^z &= \frac{1}{\Delta x^2} \left( \underline{I}_m \otimes \underline{I}_N \otimes \hat{\underline{M}}^{-1} \hat{\underline{D}}^T \underline{M} \underline{V} + \underline{P}_r^T \otimes \underline{I}_N \otimes \hat{\underline{M}}^{-1} \tilde{\underline{D}}^T \underline{M} \underline{V} \right) \underline{\overline{E}}^y \\ &\quad - \frac{1}{\Delta y^2} \left( \underline{I}_m \otimes \hat{\underline{M}}^{-1} \hat{\underline{D}}^T \underline{M} \underline{V} \otimes \underline{I}_N + \underline{P}_u^T \otimes \hat{\underline{M}}^{-1} \tilde{\underline{D}}^T \underline{M} \underline{V} \otimes \underline{I}_N \right) \underline{\overline{E}}^x. \end{aligned} \quad (110)$$

To deal with the split derivative matrix, we will denote for a  $N-1 \times N-1$  matrix  $\underline{A}$  by  $\underline{A}_{0:N-1} \in M^{N+1 \times N+1}(\mathbb{R})$  the matrix with the last row cut off and by  $\underline{A}_{N;0} \in M^{N+1 \times N+1}(\mathbb{R})$  the matrix having as first row the last row of  $\underline{A}$ , with all other entries being 0. Applying the Summation-by-Parts formula (49) now, we obtain for the first term of the left side of (110):

$$\begin{aligned}
& \frac{1}{\Delta x^2} \left( \underline{I}_m \otimes \underline{I}_N \otimes \hat{\underline{M}}^{-1} \hat{\underline{D}}^T \underline{M} \underline{V} + \underline{P}_r^T \otimes \underline{I}_N \otimes \hat{\underline{M}}^{-1} \tilde{\underline{D}}^T \underline{M} \underline{V} \right) \underline{E}^y \\
& = \frac{1}{\Delta x^2} \left( \underline{I}_m \otimes \underline{I}_N \otimes \hat{\underline{M}}^{-1} \underline{B}_{0:N-1} \underline{V} + \underline{P}_r^T \otimes \underline{I}_N \otimes \hat{\underline{M}}^{-1} \underline{B}_{N;0} \underline{V} \right) \underline{E}^y \\
& - \frac{1}{\Delta x^2} \left( \underline{I}_m \otimes \underline{I}_N \otimes \hat{\underline{M}}^{-1} \underline{M}_{0:N-1} \underline{D} \underline{V} + \underline{P}_r^T \otimes \underline{I}_N \otimes \hat{\underline{M}}^{-1} \underline{M}_{N;0} \underline{D} \underline{V} \right) \underline{E}^y. \tag{111}
\end{aligned}$$

An analogous equation holds for the second term. Component wise we obtain

$$\begin{aligned}
\frac{d}{dt} B_{k,l,m}^z & = -(1 - \delta_{0,k}) \frac{1}{\Delta x} \sum_{i=0}^N D_{k,i} E_{i,l,m}^y + \frac{1}{\Delta y} (1 - \delta_{0,l}) \sum_{i=0}^N D_{l,i} E_{k,i,m}^x \\
& - \delta_{0,k} \frac{1}{\Delta x} \frac{1}{\omega_N + \omega_0} \left( \omega_N \sum_{i=0}^N D_{N,i} E_{i,l,\sigma_{le}(m)}^y + \omega_0 \sum_{i=0}^N D_{1,i} E_{i,l,m}^y \right) \\
& + \delta_{0,l} \frac{1}{\Delta y} \frac{1}{\omega_N + \omega_0} \left( \omega_N \sum_{i=0}^N D_{N,i} E_{k,i,\sigma_{lo}(m)}^x + \omega_0 \sum_{i=0}^N D_{1,i} E_{k,i,m}^x \right) \tag{112} \\
& + \delta_{0,k} \frac{1}{\Delta x} \frac{1}{\omega_N + \omega_0} \left( E_{N,l,\sigma_{le}(m)}^y - E_{0,l,m}^y \right) \\
& - \delta_{0,l} \frac{1}{\Delta y} \frac{1}{\omega_N + \omega_0} \left( E_{k,N,\sigma_{lo}(m)}^x - E_{k,0,m}^x \right),
\end{aligned}$$

where  $E_{k,l,m}^x$  and  $E_{k,l,m}^y$  are the nodal values of the electric field computed with the scaled Vandermonde matrix while  $\sigma_{lo}(m)$  and  $\sigma_{le}(m)$  are the indices of the element below and left of the element with index  $m$ . Since we already use the scaled Vandermonde matrix in the nodal evaluation, the scaling factors in the component-wise equation are not squared anymore.

We note that on a function level, the derivative matrix  $\underline{D}$  computes the nodal derivatives of the element-local Lagrange functions, not the histopolation functions. Since we take the derivative in the directions we have the histopolation basis functions, this amounts to interpolating the functions with the element-local Lagrange basis, so without continuity requirement, and then computing the local derivative.

The strong form equation (112) then consists of the element-local interpolation derivative in x-direction for  $E^y$  and in y-direction for  $E^x$  for  $k \neq 0$  and  $l \neq 0$  respectively. If the degree of freedom in question is on the element boundary in x- or y-direction, we instead have a weighted jump penalty term minus the weighted average of the discontinuous derivative at the boundary. This results in a treatment of the discontinuous derivative similar to a finite difference SAT, a finite volume or a discontinuous Galerkin ansatz.

Proceeding from the weak formulation, we can rewrite the scheme using the discrete Hamiltonian or discrete energy defined as

$$\begin{aligned}
H(\underline{U}) & = \frac{1}{2} (\underline{E}^{x,T} \underline{V}_y^{2D,T} \underline{M}_x^{2D} \underline{V}_y^{2D} \underline{E}^x \\
& + \underline{E}^{y,T} \underline{V}_x^{2D,T} \underline{M}_y^{2D} \underline{V}_x^{2D} \underline{E}^y + \underline{B}^{z,T} \hat{\underline{M}}^{2D} \underline{B}^z), \tag{113}
\end{aligned}$$

where

$$\underline{U} = \begin{pmatrix} \underline{E}^x \\ \underline{E}^y \\ \underline{B}^z \end{pmatrix}, \quad (114)$$

and

$$\underline{J} = \begin{pmatrix} 0 & 0 & \underline{\Delta}_y^{2D} \hat{M}^{2D,-1} \\ 0 & 0 & -\underline{\Delta}_x^{2D} \hat{M}^{2D,-1} \\ -\hat{M}^{2D,-1} \underline{\Delta}_y^{2D,T} & \hat{M}^{2D,-1} \underline{\Delta}_x^{2D,T} & 0 \end{pmatrix}, \quad (115)$$

is the Poisson matrix.

Then the scheme (107), (108), and (109) is equivalent to

$$\frac{d}{dt} \underline{U} = \underline{J} \nabla_U H(\underline{U}), \quad (116)$$

with

$$\nabla_U H(\underline{U}) = \begin{pmatrix} V_y^{2D,T} M_x^{2D} V_y^{2D} \underline{E}^x \\ V_x^{2D,T} M_y^{2D} V_x^{2D} \underline{E}^y \\ \hat{M}^{2D} \underline{B}^z \end{pmatrix}. \quad (117)$$

The semi-discrete energy conservation of the scheme follows directly:

$$\frac{d}{dt} H(\underline{U}) = (\nabla_U H(\underline{U}))^T \frac{d}{dt} \underline{U} = (\nabla_U H(\underline{U}))^T \underline{J} (\nabla_U H(\underline{U})) = 0, \quad (118)$$

since  $\underline{J}$  is anti-symmetric.

#### 4.3. Time Integration

We will consider two different time integration schemes here. One is an explicit three-stage Runge-Kutta scheme [37] and the other, the discrete gradient average vector field method [38], which in this case coincides with the Crank-Nicolson scheme [39], which is implicit. The purpose of the latter is to exactly preserve the discrete energy in the fully discrete setting. The ansatz for the discrete gradient method is to find an approximation for  $\bar{\nabla}_U H(\underline{U}_n, \underline{U}_{n+1})$ , that depends on the current and the next time step, for  $\nabla H(\underline{U})$ . This approximation has to fulfill

$$(\underline{U}_{n+1} - \underline{U}_n)^T \bar{\nabla}_U H(\underline{U}_n, \underline{U}_{n+1}) = H(\underline{U}_{n+1}) - H(\underline{U}_n), \quad (119)$$

If we then define the time integration scheme implicitly by

$$\frac{1}{\Delta t} (\underline{U}_{n+1} - \underline{U}_n) = \underline{J} \bar{\nabla}_U H(\underline{U}_n, \underline{U}_{n+1}), \quad (120)$$

which conserves the Hamiltonian [38] since

$$\begin{aligned} H(\underline{U}_{n+1}) - H(\underline{U}_n) &= (\underline{U}_{n+1} - \underline{U}_n)^T \bar{\nabla}_U H(\underline{U}_n, \underline{U}_{n+1}) \\ &= \Delta t (\bar{\nabla}_U H)^T \underline{J}^T (\bar{\nabla}_U H) = 0. \end{aligned} \quad (121)$$

In this case the average vector field discrete gradient is,

$$\begin{aligned}\bar{\nabla}_U H(\underline{U}_n, \underline{U}_{n+1}) &:= \int_0^1 (\lambda \nabla_U H(\underline{U}_n) + (1 - \lambda) \nabla_U H(\underline{U}_{n+1})) d\lambda \\ &= \frac{1}{2} \nabla_U H(\underline{U}_{n+1} + \underline{U}_n).\end{aligned}\quad (122)$$

Since  $\nabla_U H$  is linear, this choice leads to the Crank-Nicolson time integration method [39]:

$$\frac{1}{\Delta t} (\underline{U}_{n+1} - \underline{U}_n) = \frac{1}{2} \underline{J} \nabla_U H(\underline{U}_{n+1} + \underline{U}_n). \quad (123)$$

**Proposition 1.** *Both the Crank-Nicolson method and any Runge-Kutta scheme applied to the semi-discrete method given by (107), (108) and (109) exactly preserve the divergence of the electric field in time. If the divergence was 0 at the start time  $t_0$ , it remains 0 at all time-steps  $t_n$ .*

*Proof.* The update step for a  $s$ -stage Runge-Kutta scheme for the electric field has the form

$$\begin{pmatrix} \bar{E}_n^x \\ \bar{E}_n^y \\ \bar{E}_n^z \end{pmatrix} = \begin{pmatrix} \bar{E}_n^x \\ \bar{E}_n^y \\ \bar{E}_n^z \end{pmatrix} + \Delta t \begin{pmatrix} \Delta_x^{2D} \\ \Delta_y^{2D} \\ -\Delta_x^{2D} \end{pmatrix} \sum_{j=1}^s \begin{pmatrix} k_j^x \\ k_j^y \\ k_j^z \end{pmatrix}, \quad (124)$$

for vectors  $k_j^x$  and  $k_j^y$  that are generally dependent on all other stages of the Runge-Kutta scheme. Applying the discrete divergence on both sides yields

$$\begin{aligned}\begin{pmatrix} \Delta_x^{2D} \\ \Delta_y^{2D} \end{pmatrix} \cdot \begin{pmatrix} \bar{E}_n^x \\ \bar{E}_n^y \\ \bar{E}_n^z \end{pmatrix} &= \begin{pmatrix} \Delta_x^{2D} \\ \Delta_y^{2D} \end{pmatrix} \cdot \begin{pmatrix} \bar{E}_n^x \\ \bar{E}_n^y \\ \bar{E}_n^z \end{pmatrix} \\ &+ \Delta t \begin{pmatrix} \Delta_x^{2D} \\ \Delta_y^{2D} \end{pmatrix} \cdot \begin{pmatrix} \Delta_x^{2D} \\ \Delta_y^{2D} \\ -\Delta_x^{2D} \end{pmatrix} \sum_{j=1}^s k_j = \begin{pmatrix} \Delta_x^{2D} \\ \Delta_y^{2D} \end{pmatrix} \cdot \begin{pmatrix} \bar{E}_n^x \\ \bar{E}_n^y \\ \bar{E}_n^z \end{pmatrix}\end{aligned}\quad (125)$$

where we used (102). For the Crank-Nicolson method we have

$$\frac{1}{\Delta t} \left( \begin{pmatrix} \bar{E}_n^x \\ \bar{E}_n^y \\ \bar{E}_n^z \end{pmatrix} - \begin{pmatrix} \bar{E}_{n+1}^x \\ \bar{E}_{n+1}^y \\ \bar{E}_{n+1}^z \end{pmatrix} \right) = \frac{1}{2} \underline{J} \nabla_U H \left( \begin{pmatrix} \bar{E}_n^x \\ \bar{E}_n^y \\ \bar{E}_n^z \end{pmatrix} + \begin{pmatrix} \bar{E}_{n+1}^x \\ \bar{E}_{n+1}^y \\ \bar{E}_{n+1}^z \end{pmatrix} \right). \quad (126)$$

Applying the discrete divergence to the electric field yields

$$\frac{1}{\Delta t} \begin{pmatrix} \Delta_x^{2D} \\ \Delta_y^{2D} \\ 0 \end{pmatrix} \cdot \left( \begin{pmatrix} \bar{E}_n^x \\ \bar{E}_n^y \\ \bar{E}_n^z \end{pmatrix} - \begin{pmatrix} \bar{E}_{n+1}^x \\ \bar{E}_{n+1}^y \\ \bar{E}_{n+1}^z \end{pmatrix} \right) = 0, \quad (127)$$

or

$$\begin{pmatrix} \Delta_x^{2D} \\ \Delta_y^{2D} \\ 0 \end{pmatrix} \cdot \begin{pmatrix} \bar{E}_n^x \\ \bar{E}_n^y \\ \bar{E}_n^z \end{pmatrix} = \begin{pmatrix} \Delta_x^{2D} \\ \Delta_y^{2D} \\ 0 \end{pmatrix} \cdot \begin{pmatrix} \bar{E}_{n+1}^x \\ \bar{E}_{n+1}^y \\ \bar{E}_{n+1}^z \end{pmatrix}, \quad (128)$$

which completes the proof.  $\square$

## 5. Numerical Verification

We look at the test case from [40] with domain  $\Omega = [-1, 1]^2$ , end time  $T = 1$ , and the initial condition

$$E^x(x, y) = 0, \quad (129)$$

$$E^y(x, y) = 0, \quad (130)$$

$$B^z(x, y) = \cos(\pi x + \pi) \cos(\pi y + \pi), \quad (131)$$

with the analytical solution

$$E^x(x, y) = -\frac{1}{\sqrt{2}} \cos(\pi x + \pi) \sin(\pi y + \pi) \sin(\sqrt{2}\pi t), \quad (132)$$

$$E^y(x, y) = \frac{1}{\sqrt{2}} \sin(\pi x + \pi) \cos(\pi y + \pi) \sin(\sqrt{2}\pi t), \quad (133)$$

$$B^z(x, y) = \cos(\pi x + \pi) \cos(\pi y + \pi) \cos(\sqrt{2}\pi t). \quad (134)$$

For our tests we use a Julia code, using scripts from [32]. To solve the linear system for the Crank-Nicolson method, we use the GMRES solver [41] implemented in the Julia package Krylov.jl [42]. For the repository, see the data availability section. The tests are run with Julia 1.11.7 on Ubuntu 24.04.3 LTS with a AMD Ryzen 9 9900X processor.

### 5.1. Convergence Tests

We run two different kinds of convergence tests, where we use the discrete  $L^2$  norm induced by our global mass matrices. For the first kind of convergence test we keep the number of points per element constant but varying the amount of elements. For time integration we use a three-stage strong stability-preserving Runge-Kutta scheme (see [37], equation (2.18)) with a constant time step of  $\Delta t = 2 \cdot 10^{-5}$ . We run this test for operators of boundary order 2 and 3 by Strand [26] several times, varying the amount of points per element between test sets, to both include operators containing only the boundary stencils and operators mostly containing inner stencils.

For both polynomial degrees we observe an even-odd behavior in figures 6-11, where we obtain an alternating order of  $p$  and  $p + 1$  for the electric field, depending on the number of points per element. This behavior is documented for central schemes, see for instance [43]. For the magnetic field the order is more erratic, nonetheless do we obtain an average EOC close to  $p+1$ . The second kind of test is again run using operators from [26] of polynomial degrees 2 and 3. The time integration this time is now performed using the same SSPRK scheme from the first tests, but also with the energy-conservative Crank-Nicolson scheme. We again use a constant time step of  $\Delta t = 2 \cdot 10^{-5}$ . For the spatial discretization we just use one element, but a varying amount of nodes per element. In figures 12-15 we see higher polynomial orders than in the first test, which is likely due to the fact that the inner stencils, which are of degree  $2p$  become more influential and increase the EOC.

Number of Elements	$E^x/E^y$ Error	$E^x/E^y$ EOC	$B^z$ Error	$B^z$ EOC
1	$1.487802e - 1$	-	$2.128334e - 1$	-
2	$1.457635e - 2$	3.35	$3.770852e - 2$	2.50
4	$3.215945e - 3$	2.18	$2.840422e - 3$	3.73
8	$4.087012e - 4$	2.98	$2.402008e - 4$	3.56
16	$4.357807e - 5$	3.23	$4.276273e - 5$	2.49
32	$5.590312e - 6$	2.96	$8.925102e - 6$	2.26

Figure 6: Discrete  $L^2$ -Errors and EOC for degree  $p = 2$  with 8 points per direction per element

### 5.2. Divergence Tests

A key property of the proposed discretization is the exact preservation of the divergence condition (55). We test this using both a coarse discretization using 2 elements with 12 points and a finer discretization using 5 elements with 20 points in each direction. For the coarse discretization we also simulate up to the end time  $T = 10000$ . We again test the divergence preservation with the operators of degree 2 and 3 and both with the SSPRK and the Crank-Nicolson scheme. The time step is defined by

$$\Delta t = \text{CFL } \omega_{min}, \quad (135)$$

for  $\text{CFL} = 1$ . Here  $\omega_{min}$  is the minimal quadrature weight of the global mass matrix  $\hat{M}_{2D}$ . The figures 16, 17 and 18 show the maximum absolute value of the divergence of the electric field at the grid points. We can observe that the solution remains divergence free up to machine precision during the entire simulation, regardless of operator, time integration scheme, or grid size. The rounding errors for the SSPRK scheme do not increase anymore after a certain time, which is due to the fact that the energy has almost completely dissipated away. This confirms the previously proven fully discrete divergence preservation.

### 5.3. Energy Conservation Tests

We repeat the tests performed for divergence preservation to test the conservation of energy over time. We use the same operators and the same time integration schemes with the grid sizes. In figures 19, 20 and 21 we plot the difference between the discrete energy at  $t = 0$  and the energy at the given point in time. We can observe that the SSPRK is energy dissipative and does not conserve the energy exactly. This effect lessens for the finer grid size, but is still present. On the other hand the Crank Nicolson time integration method conserves the energy exactly as proven previously.

Number of Elements	$E^x/E^y$ Error	$E^x/E^y$ EOC	$B^z$ Error	$B^z$ EOC
1	$9.964855e - 2$	-	$1.260615e - 1$	-
2	$1.130372e - 2$	3.14	$5.891993e - 3$	4.42
4	$2.212383e - 3$	2.35	$1.149555e - 3$	2.36
8	$5.62475e - 4$	1.98	$1.331211e - 4$	3.11
16	$1.407649e - 4$	2	$5.033169e - 6$	4.73
32	$3.518716e - 5$	2	$1.586997e - 6$	1.67

Figure 7: Discrete  $L^2$ -Errors and EOC for degree  $p = 2$  with 9 points per direction per element

Number of Elements	$E^x/E^y$ Error	$E^x/E^y$ EOC	$B^z$ Error	$B^z$ EOC
1	$4.418904e - 2$	-	$1.054903e - 1$	-
2	$3.740646e - 3$	3.56	$1.440109e - 2$	2.87
4	$1.34654e - 3$	1.47	$1.170316e - 3$	3.62
8	$1.722958e - 4$	2.97	$2.350005e - 4$	2.32
16	$2.678038e - 5$	2.69	$1.035082e - 5$	4.5
32	$2.699576e - 6$	3.31	$2.375989e - 6$	2.12

Figure 8: Discrete  $L^2$ -Errors and EOC for degree  $p = 2$  with 10 points per direction per element

Number of Elements	$E^x/E^y$ Error	$E^x/E^y$ EOC	$B^z$ Error	$B^z$ EOC
1	$1.566639e - 2$	-	$2.98044e - 2$	-
2	$2.159529e - 3$	2.86	$5.705334e - 3$	2.39
4	$2.37442e - 4$	3.19	$6.683885e - 5$	6.42
8	$1.55675e - 5$	3.93	$5.264376e - 6$	3.67
16	$1.795338e - 6$	3.12	$5.574813e - 7$	3.24
32	$2.215563e - 7$	3.02	$2.440927e - 8$	4.51

Figure 9: Discrete  $L^2$ -Errors and EOC for degree  $p = 3$  with 12 points per direction per element

Number of Elements	$E^x/E^y$ Error	$E^x/E^y$ EOC	$B^z$ Error	$B^z$ EOC
1	$1.487912e - 2$	-	$2.082052e - 2$	-
2	$2.703255e - 3$	2.46	$5.469707e - 4$	5.25
4	$1.58823e - 4$	4.09	$4.118751e - 5$	3.73
8	$7.39334e - 6$	4.43	$5.613232e - 6$	2.88
16	$4.856478e - 7$	3.93	$8.610113e - 8$	6.03
32	$2.558402e - 8$	4.25	$2.16185e - 8$	1.99

Figure 10: Discrete  $L^2$ -Errors and EOC for degree  $p = 3$  with 13 points per direction per element

Number of Elements	$E^x/E^y$ Error	$E^x/E^y$ EOC	$B^z$ Error	$B^z$ EOC
1	$8.506095e - 3$	-	$2.235792e - 2$	-
2	$9.643637e - 4$	3.14	$3.285374e - 3$	2.77
4	$1.017081e - 4$	3.25	$4.232642e - 5$	6.28
8	$7.697999e - 6$	3.72	$4.7801012e - 6$	3.15
16	$9.530514e - 7$	3.01	$1.958355e - 7$	4.61
32	$1.176027e - 7$	3.02	$1.007924e - 8$	4.28

Figure 11: Discrete  $L^2$ -Errors and EOC for degree  $p = 3$  with 14 points per direction per element

Points per Element	$E^x/E^y$ Error	$E^x/E^y$ EOC	$B^z$ Error	$B^z$ EOC
8	$1.487802e - 1$	-	$2.128334e - 1$	-
16	$9.078998e - 3$	4.03	$1.586406e - 2$	3.75
32	$4.807838e - 4$	4.24	$8.52153e - 4$	4.22
64	$3.536512e - 5$	3.76	$4.897816e - 5$	4.12
128	$2.885322e - 6$	3.62	$2.921983e - 6$	4.07
256	$2.459519e - 7$	3.55	$1.785489e - 7$	4.03

Figure 12: Discrete  $L^2$ -Errors and EOC for degree  $p = 2$  with SSPRK time integration with varying points per element

Points per Element	$E^x/E^y$ Error	$E^x/E^y$ EOC	$B^z$ Error	$B^z$ EOC
12	$1.566639e - 2$	-	$2.98044e - 2$	-
24	$1.16444e - 3$	3.75	$3.248053e - 3$	3.2
48	$9.278422e - 5$	3.65	$1.437682e - 4$	4.5
96	$5.909218e - 6$	3.97	$6.813822e - 6$	4.4
192	$3.838066e - 7$	3.94	$2.919607e - 7$	4.54
384	$2.347673e - 8$	4.03	$1.309507e - 8$	4.48

Figure 13: Discrete  $L^2$ -Errors and EOC for degree  $p = 3$  with SSPRK time integration with varying points per element

Points per Element	$E^x/E^y$ Error	$E^x/E^y$ EOC	$B^z$ Error	$B^z$ EOC
8	$1.487802e - 1$	-	$2.128334e - 1$	-
16	$9.078998e - 3$	4.03	$1.586407e - 2$	3.75
32	$4.807839e - 4$	4.24	$8.521539e - 4$	4.22
64	$3.536516e - 5$	3.76	$4.897902e - 5$	4.12
128	$2.885341e - 6$	3.62	$2.922832e - 6$	4.07
256	$2.459736e - 7$	3.55	$1.794117e - 7$	4.03

Figure 14: Discrete  $L^2$ -Errors and EOC for degree  $p = 2$  with Crank-Nicolson time integration with varying points per element

Points per Element	$E^x/E^y$ Error	$E^x/E^y$ EOC	$B^z$ Error	$B^z$ EOC
12	$1.566639e - 2$	-	$2.98044e - 2$	-
24	$1.16444e - 3$	3.75	$3.248053e - 3$	3.2
48	$9.278422e - 5$	3.65	$1.437682e - 4$	4.5
96	$5.909218e - 6$	3.97	$6.813825e - 6$	4.4
192	$3.838071e - 7$	3.94	$2.919745e - 7$	4.54
384	$2.348321e - 8$	4.03	$1.339557e - 8$	4.45

Figure 15: Discrete  $L^2$ -Errors and EOC for degree  $p = 3$  with Crank-Nicolson time integration with varying points per element

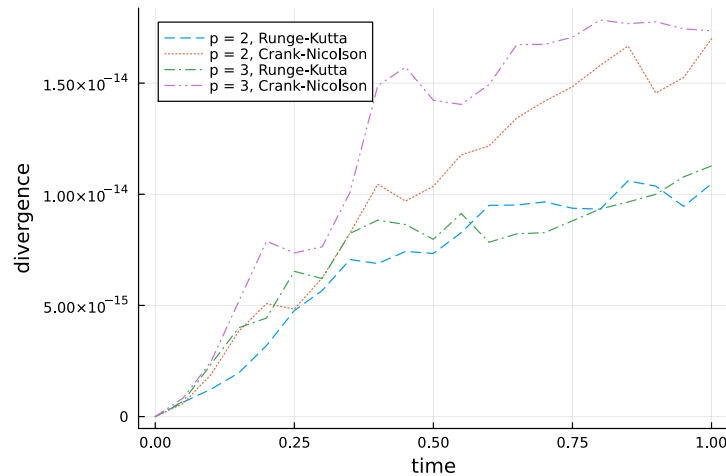


Figure 16: Divergence errors for operators of degree  $p = 2, 3$  with both the SSPRK and Crank-Nicolson time integration, 2 elements with 12 points per dimension

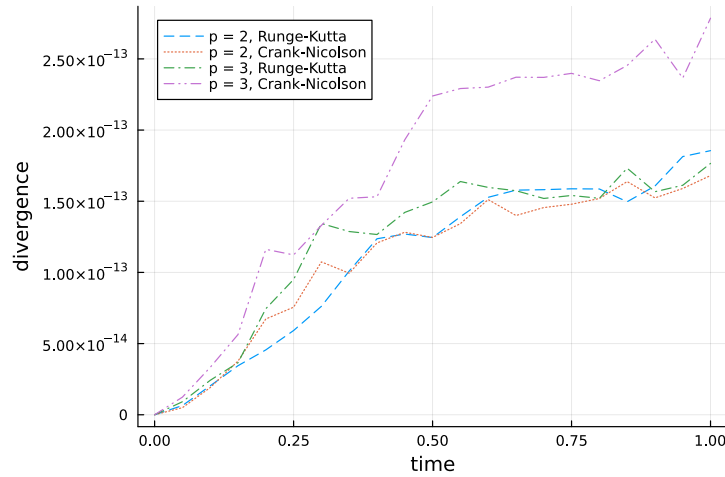


Figure 17: Divergence errors for operators of degree  $p = 2, 3$  with both the SSPRK and Crank-Nicolson time integration, 5 elements with 20 points per dimension

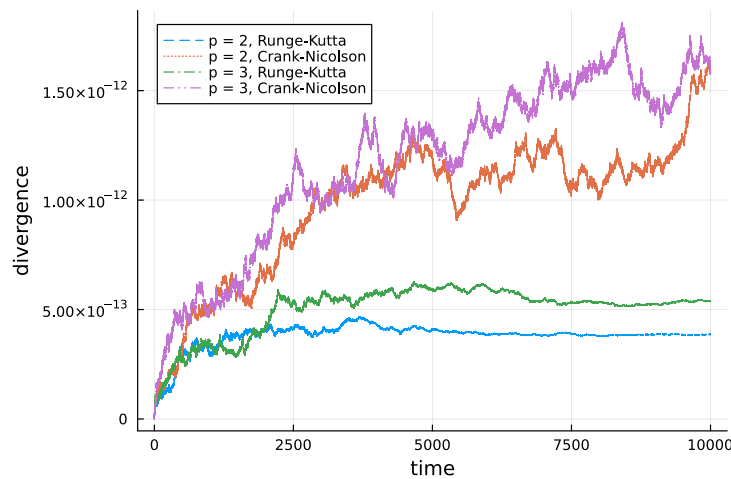


Figure 18: Divergence errors for operators of degree  $p = 2, 3$  with both the SSPRK and Crank-Nicolson time integration, 2 elements with 12 points per dimension, end time  $T = 10000$

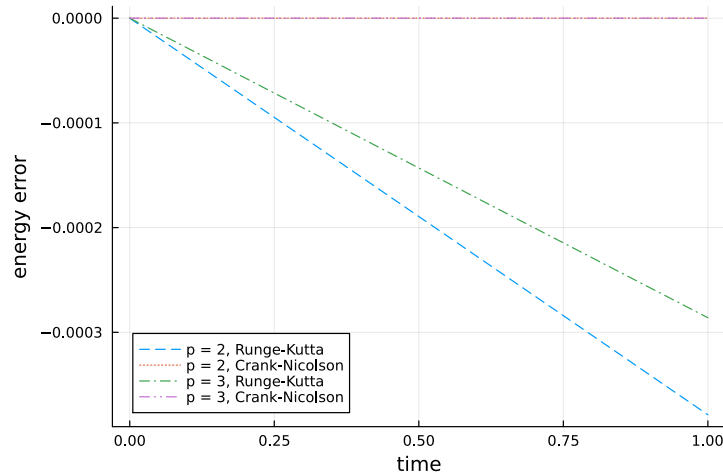


Figure 19: Energy errors for operators of degree  $p = 2, 3$  with both the SSPRK and Crank-Nicolson time integration, 2 elements with 12 points per dimension

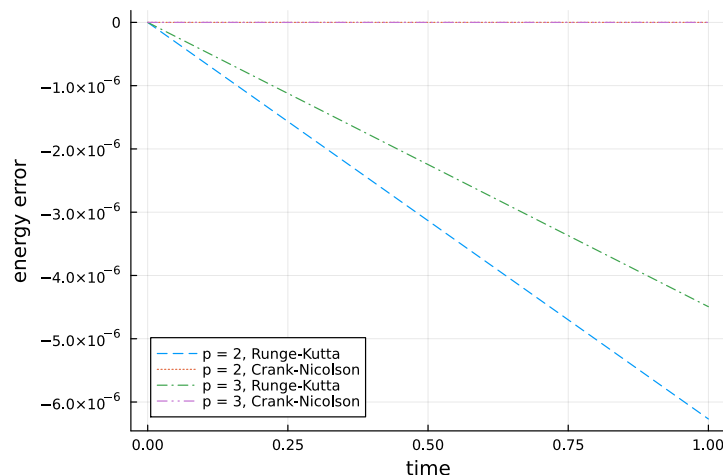


Figure 20: Energy errors for operators of degree  $p = 2, 3$  with both the SSPRK and Crank-Nicolson time integration, 5 elements with 20 points per dimension

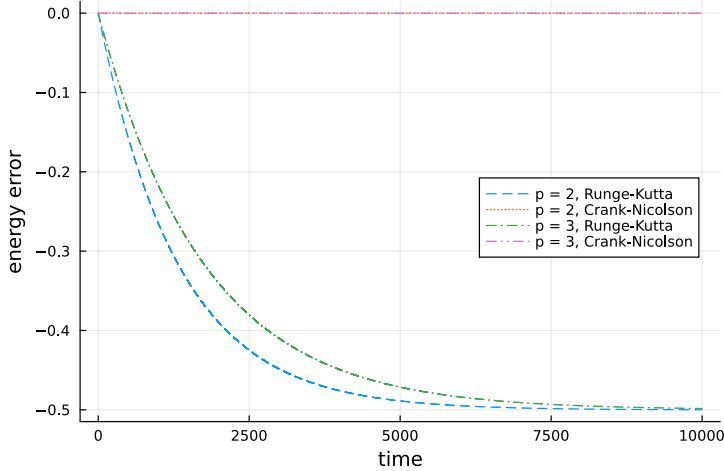


Figure 21: Energy errors for operators of degree  $p = 2, 3$  with both the SSPRK and Crank-Nicolson integration, 2 elements with 12 points per dimension, end time  $T = 10000$

## 6. Conclusion

Using the theory of Finite Element Exterior Calculus [1, 2], we derived a family of divergence preserving and semi-discretely energy-conservative schemes for the homogeneous transverse electric Maxwell's equations using pre-existing SBP-FD operators. Using the Summation-by-Parts property we derived a strong form formulation of our semi-discretization from the weakly discretized Faraday's law, analogously to other SBP schemes such as the DGSEM [35]. To derive the scheme, we extended the construction by Gerritsma et al. [16, 17] using nodal and integral degrees of freedom. Instead of permitting only polynomial basis functions however, we derived the compatible spaces using more general basis functions, that we only require to have the Lagrange property and the correct derivative values on the grid nodes of the SBP operator. This allows us to substitute any SBP-FD operator to derive our SBP-FDEC scheme. Since we extended our approach to 2D and 3D using a tensor product ansatz, we were able to derive general representations for the derivative operators of the 2D and 3D de Rham complexes, yielding commuting discrete complexes, for any given SBP-FD operators, similar to [16], making the scheme easily extendable to 3D.

Using standard energy-conservative time integration schemes, we can use the semi-discrete energy conservation to derive a fully discrete energy-conservative scheme. Further we were able to prove the semi-discrete and discrete divergence preserving and the energy conservative properties of our schemes. We validated our approach with a periodic test case, using SBP-FD operators by Strand [26], demonstrating both the expected order of convergence, the discrete divergence preserving property and for the Crank-Nicolson time integration method the discrete energy-conservation of our schemes.

## Declarations

*Conflicts of Interest.* The authors declare that there are no conflicts of interest.

*CrediT authorship contribution statement.* Daniel Bach: Investigation, Methodology, Formal Analysis, Software, Writing – original draft, Writing – review & editing. Andrés M. Rueda-Ramírez: Investigation, Methodology, Software, Writing – review & editing. Eric Sonnendrücker: Writing – review & editing. David C. Del Rey Fernandez: Writing – review & editing. Gregor Gassner: Conceptualization, Investigation, Writing – original draft, Writing – review & editing, Funding acquisition, Project administration.

*Data Availability.* A reproducibility repository can be accessed under [https://github.com/amrueda/paper\\_2025\\_sbp\\_fdec](https://github.com/amrueda/paper_2025_sbp_fdec)

*Funding.* Gregor Gassner and Andrés M. Rueda-Ramírez acknowledge funding through the Klaus-Tschira Stiftung via the project “HiFiLab” (00.014.2021) and through the German Federal Ministry for Education and Research (BMBF) project “ICON-DG” (01LK2315B) of the “WarmWorld Smarter” program.

Gregor Gassner and Daniel Bach acknowledge funding from the German Science Foundation DFG through the research unit “SNuBIC” (DFG-FOR5409).

Andrés M. Rueda-Ramírez gratefully acknowledges funding from the Spanish Ministry of Science, Innovation, and Universities through the “Beatrix Galindo” grant BG23-00062 and from the European Research Council through the Synergy Grant Agreement No. 101167322-TRANSDIFFUSE.

## References

- [1] D. Arnold, R. Falk, R. Winther, Finite element exterior calculus, homological techniques, and applications, *Acta Numerica* 15 (2006) 1–155. doi:<https://doi.org/10.1017/S0962492906210018>.
- [2] D. Arnold, R. Falk, R. Winther, Finite element exterior calculus: from Hodge theory to numerical stability, *Bulletin of the American Mathematical Society* 47(2) (2010) 281–354. doi:<https://doi.org/10.1090/S0273-0979-10-01278-4>.
- [3] D. N. Arnold, Finite Element Exterior Calculus, Society for Industrial and Applied Mathematics, Philadelphia, PA, 2018. arXiv:<https://pubs.siam.org/doi/pdf/10.1137/1.9781611975543>, doi:10.1137/1.9781611975543.
- [4] P. Monk, Finite Element Methods for Maxwell’s Equations, Oxford University Press, 2003. doi:10.1093/acprof:oso/9780198508885.001.0001.
- [5] M. Kraus, K. Kormann, P. J. Morrison, E. Sonnendrücker, Gempic: geometric electromagnetic particle-in-cell methods, *Journal of Plasma Physics* 83 (4) (2017) 905830401. doi:10.1017/S002237781700040X.

- [6] M. Campos Pinto, K. Kormann, E. Sonnendrücker, Variational framework for structure-preserving electromagnetic particle-in-cell methods, *Journal of Scientific Computing* 91 (46) (2022).
- [7] A. Palha, M. Gerritsma, A mass, energy, enstrophy and vorticity conserving (meevc) mimetic spectral element discretization for the 2d incompressible navier–stokes equations, *Journal of Computational Physics* 328 (2017) 200–220. doi:<https://doi.org/10.1016/j.jcp.2016.10.009>.
- [8] V. Carlier, M. Campos Pinto, F. Fambri, Mass, momentum and energy preserving feec and broken-feec schemes for the incompressible navier–stokes equations, *IMA Journal of Numerical Analysis* 45 (3) (2024) 1868–1904. doi:[10.1093/imanum/drae047](https://doi.org/10.1093/imanum/drae047).
- [9] Y. Güçlü, S. Hadjout, M. Campos Pinto, A broken feec framework for electromagnetic problems on mapped multipatch domains, *Journal of Scientific Computing* 97 (2) (2023) 52.
- [10] J. C. Nédélec, Mixed finite elements in  $\mathbb{R}^3$ , *Numerische Mathematik* 35 (1980) 315–341. doi:<https://doi.org/10.1007/BF01396415>.
- [11] J. C. Nédélec, A new family of mixed finite elements in  $\mathbb{R}^3$ , *Numerische Mathematik* 50 (1986) 57–81. doi:<https://doi.org/10.1007/BF01389668>.
- [12] H. Whitney, *Geometric Integration Theory*, Princeton University Press, Princeton, 1957. doi:<https://doi.org/10.1515/9781400877577>.
- [13] P. A. Raviart, J. M. Thomas, A mixed finite element method for 2-nd order elliptic problems, in: I. Galligani, E. Magenes (Eds.), *Mathematical Aspects of Finite Element Methods*, Springer Berlin Heidelberg, Berlin, Heidelberg, 1977, pp. 292–315. doi:<https://doi.org/10.1007/BFb0064470>.
- [14] A. Buffa, C. de Falco, G. Sangalli, Isogeometric analysis: Stable elements for the 2D stokes equation, *International Journal for Numerical Methods in Fluids* 65 (11-12) (2011) 1407–1422. doi:<https://doi.org/10.1002/fld.2337>.
- [15] J. A. Evans, T. J. Hughes, Isogeometric divergence-conforming b-splines for the unsteady navier–stokes equations, *Journal of Computational Physics* 241 (2013) 141–167. doi:<https://doi.org/10.1016/j.jcp.2013.01.006>.
- [16] M. Gerritsma, Edge Functions for Spectral Element Methods, in: J. S. Hesthaven, E. M. Rønquist (Eds.), *Spectral and High Order Methods for Partial Differential Equations*, Springer Berlin Heidelberg, Berlin, Heidelberg, 2011, pp. 199–207. doi:[https://doi.org/10.1007/978-3-642-15337-2\\_17](https://doi.org/10.1007/978-3-642-15337-2_17).
- [17] J. Kreeft, A. Palha, M. Gerritsma, Mimetic framework on curvilinear quadrilaterals of arbitrary order (2011). doi:<https://doi.org/10.48550/arXiv.1111.4304>.

- [18] K. Lipnikov, G. Manzini, M. Shashkov, Mimetic finite difference method, *Journal of Computational Physics* 257 (2014) 1163–1227, physics-compatible numerical methods. doi:<https://doi.org/10.1016/j.jcp.2013.07.031>.
- [19] A. A. Samarskii, *The Theory of Difference Schemes*, CSC Press, 2001.
- [20] K. Yee, Numerical solution of initial boundary value problems involving maxwell's equations in isotropic media, *IEEE Transactions on Antennas and Propagation* 14 (3) (1966) 302–307. doi:<https://doi.org/10.1109/TAP.1966.1138693>.
- [21] J. M. Hyman, M. Shashkov, Adjoint operators for the natural discretizations of the divergence, gradient and curl on logically rectangular grids, *Applied Numerical Mathematics* 25 (4) (1997) 413–442. doi:[https://doi.org/10.1016/S0168-9274\(97\)00097-4](https://doi.org/10.1016/S0168-9274(97)00097-4).
- [22] J. Hyman, M. Shashkov, Natural discretizations for the divergence, gradient, and curl on logically rectangular grids, *Computers & Mathematics with Applications* 33 (4) (1997) 81–104. doi:[https://doi.org/10.1016/S0898-1221\(97\)00009-6](https://doi.org/10.1016/S0898-1221(97)00009-6).
- [23] J. Hyman, M. Shashkov, Approximation of boundary conditions for mimetic finite-difference methods, *Computers & Mathematics with Applications* 36 (5) (1998) 79–99. doi:[https://doi.org/10.1016/S0898-1221\(98\)00152-7](https://doi.org/10.1016/S0898-1221(98)00152-7).
- [24] K. Kormann, E. Sonnendrücker, A dual grid geometric electromagnetic particle in cell method, *SIAM Journal on Scientific Computing* 46 (5) (2024) B621–B646.
- [25] H.-O. Kreiss, G. Scherer, *Finite Element and Finite Difference Methods for Hyperbolic Partial Differential Equations*, Elsevier, 1974, pp. 195–212. doi:<https://doi.org/10.1016/B978-0-12-208350-1.50012-1>.
- [26] B. Strand, Summation by parts for finite difference approximations for  $d/dx$ , *Journal of Computational Physics* 110 (1) (1994) 47–67. doi:<https://doi.org/10.1006/jcph.1994.1005>.
- [27] P. Olsson, Summation by parts, projections, and stability. i, *Mathematics of Computation* 64 (211) (1995) 1035 – 1065. doi:<https://doi.org/10.1090/S0025-5718-1995-1297474-X>.
- [28] P. Olsson, Summation by parts, projections, and stability. ii, *Mathematics of Computation* 64 (212) (1995) 1473 – 1493. doi:<https://doi.org/10.1090/S0025-5718-1995-1308459-9>.
- [29] J. Crean, J. E. Hicken, D. C. Del Rey Fernández, D. W. Zingg, M. H. Carpenter, Entropy-stable summation-by-parts discretization of the euler equations on general curved elements, *Journal of Computational Physics* 356 (2018) 410–438. doi:<https://doi.org/10.1016/j.jcp.2017.12.015>.

- [30] M. H. Carpenter, M. Parsani, E. J. Nielsen, T. C. Fisher, Towards an Entropy Stable Spectral Element Framework for Computational Fluid Dynamics. arXiv:<https://arc.aiaa.org/doi/pdf/10.2514/6.2016-1058>, doi:<https://doi.org/10.2514/6.2016-1058>.
- [31] M. Svärd, J. Nordström, Review of summation-by-parts schemes for initial-boundary-value problems, *Journal of Computational Physics* 268 (2014) 17–38. doi:<https://doi.org/10.1016/j.jcp.2014.02.031>.
- [32] D. C. D. R. Fernández, J. E. Hicken, D. W. Zingg, Review of summation-by-parts operators with simultaneous approximation terms for the numerical solution of partial differential equations, *Computers & Fluids* 95 (2014) 171–196. doi:<https://doi.org/10.1016/j.compfluid.2014.02.016>.
- [33] J. Glaubitz, J. Nordström, P. Öffner, Summation-by-parts operators for general function spaces, *SIAM Journal on Numerical Analysis* 61 (2) (2023) 733–754. doi:<https://doi.org/10.1137/22M1470141>.
- [34] Glaubitz ,Jan and Klein, Simon-Christian and Nordström, Jan and Öffner, Philipp, Summation-by-parts operators for general function spaces: The second derivative, *Journal of Computational Physics* 504 (2024) 112889. doi:<https://doi.org/10.1016/j.jcp.2024.112889>.  
URL <https://www.sciencedirect.com/science/article/pii/S0021999124001384>
- [35] D. A. Kopriva, Metric Identities and the Discontinuous Spectral Element Method on Curvilinear Meshes, *Journal of Scientific Computing* 26 (2006) 301–327. doi:<https://doi.org/10.1007/s10915-005-9070-8>.
- [36] G. Gassner, A skew-symmetric discontinuous Galerkin spectral element discretization and its relation to SBP-SAT finite difference methods, *SIAM Journal on Scientific Computing* 35 (3) (2013) A1233–A1253.
- [37] C.-W. Shu, S. Osher, Efficient implementation of essentially non-oscillatory shock-capturing schemes, *Journal of computational physics* 77 (2) (1988) 439–471. doi:[https://doi.org/10.1016/0021-9991\(88\)90177-5](https://doi.org/10.1016/0021-9991(88)90177-5).
- [38] R. I. McLachlan, G. Quispel, N. Robidoux, Geometric integration using discrete gradients, *Philosophical Transactions of the Royal Society A: Mathematical, Physical and Engineering Sciences* 357 (1999) 1021–1045. doi:<https://doi.org/10.1098/rsta.1999.0363>.
- [39] C. J., N. P., A practical method for numerical evaluation of solutions of partial differential equations of the heat-conduction type, *Mathematical Proceedings of the Cambridge Philosophical Society* 43(1) (1947) 50–67. doi:<https://doi.org/10.1017/S0305004100023197>.
- [40] A. Ratnani, E. Sonnendrücker, High-Order Spline Finite Element Solver for the Time Domain Maxwell Equations, *Journal of Scientific Computing* 51 (2012) 87–106. doi:<https://doi.org/10.1007/s10915-011-9500-8>.

- [41] Y. Saad, M. Schultz, Gmres: A generalized minimal residual algorithm for solving nonsymmetric linear systems, *SIAM Journal on Scientific and Statistical Computing* 7(3) (1986) 856–869. doi:<https://doi.org/10.1137/0907058>.
- [42] A. Montoison, D. Orban, Krylov.jl: A Julia basket of hand-picked Krylov methods, *Journal of Open Source Software* 8 (89) (2023) 5187. doi:<https://doi.org/10.21105/joss.05187>.
- [43] F. J. Hindenlang, G. J. Gassner, On the Order Reduction of Entropy Stable DGSEM for the Compressible Euler Equations, in: S. J. Sherwin, D. Moxey, J. Peiró, P. E. Vincent, C. Schwab (Eds.), *Spectral and High Order Methods for Partial Differential Equations ICOSAHOM 2018*, Springer International Publishing, Cham, 2020, pp. 21–44. doi:[https://doi.org/10.1007/978-3-030-39647-3\\_2](https://doi.org/10.1007/978-3-030-39647-3_2).